# CHAPTER 43
# THE OPTICAL PROPERTIES OF WATER

**Curtis D. Mobley**
*Senior Research Engineer*
*Applied Electromagnetics and Optics Laboratory*
*SRI International*
*Menlo Park, California*

## 43.1 INTRODUCTION

This article discusses the optical properties of three substances: pure water, pure sea water, and natural water. Pure water (i.e. water molecules only) without any dissolved substances, ions, bubbles, or other impurities, is exceptionally difficult to produce in the laboratory. For this and other reasons, definitive direct measurements of its optical properties at visible wavelengths have not yet been made. Pure sea water—pure water plus various dissolved salts—has optical properties close to those of pure water. Neither pure water nor pure sea water ever occur in nature. Natural waters, both fresh and saline, are a witch's brew of dissolved and particulate matter. These solutes and particulates are both optically significant and highly variable in kind and concentration. Consequently, the optical properties of natural waters show large temporal and spatial variations and seldom resemble those of pure water.

The great variability of the optical properties of natural water is the bane of those who desire precise and easily tabulated data. However, it is the connections between the optical properties and the biological, chemical, and geological constituents of natural water and the physical environment that define the critical role of optics in aquatic research. For just as optics utilizes results from the biological, chemical, geological, and physical subdisciplines of limnology and oceanography, so do those subdisciplines incorporate optics. This synergism is seen in such areas as bio-optical oceanography, marine photochemistry, mixed-layer dynamics, laser bathymetry, and remote sensing of biological productivity, sediment load, or pollutants.

## 43.2 TERMINOLOGY, NOTATION, AND DEFINITIONS

*Hydrologic optics* is the quantitative study of the interactions of radiant energy with the earth's oceans, estuaries, lakes, rivers, and other water bodies. Most past and current

research within hydrologic optics has been within the subfield of oceanic optics, in particular the optics of deep ocean waters, as opposed to coastal or estuarine areas. This emphasis is reflected in our uneven understanding of the optical properties of various water types.

Although the optical properties of different water bodies can vary greatly, there is an overall similarity that is quite distinct from, say, the optical properties of the atmosphere. Therefore, hydrologic and atmospheric optics have developed considerably different theoretical formulations, experimental methodologies, and instrumentation as suited to each field's specific scientific issues. Chapter 44, by Killinger et al., in this *Handbook* discusses atmospheric optics. The text by Mobley[1] gives a comprehensive treatment of hydrologic optics.

Radiative transfer theory is the framework that connects the optical properties of water with the ambient light field. A rigorous mathematical formulation of radiative transfer theory as applicable to hydrologic optics has been developed by Preisendorfer[2] and others. Preisendorfer found it convenient to divide the optical properties of water into two classes: inherent and apparent. *Inherent optical properties* (IOPs) are those properties that depend only upon the medium and therefore are independent of the ambient light field within the medium. The two fundamental IOPs are the absorption coefficient and the volume scattering function. Other IOPs include the attenuation coefficient and the single-scattering albedo. *Apparent optical properties* (AOPs) are those properties that depend both on the medium (the IOPs) and on the geometric (directional) structure of the ambient light field and that display enough regular features and stability to be useful descriptors of the water body. Commonly used AOPs are the irradiance reflectance, the average cosines, and the various attenuation functions (K functions). (All of these quantities are defined below.) The radiative transfer equation provides the connection between the IOPs and the AOPs. The physical environment of a water body—waves on its surface, the character of its bottom, the incident radiance from the sky—enters the theory via the boundary conditions necessary for solution of the radiative transfer equation.

The IOPs are easily defined but they can be exceptionally difficult to measure, especially in situ. The AOPs are generally much easier to measure, but they are difficult to interpret because of the confounding environmental effects. (A change in the sea surface wave state or in the sun's position changes the radiance distribution, and hence the AOPs, even though the IOPs are unchanged.)

Hydrologic optics employs standard radiometric concepts and terminology, although the notation adopted by the International Association for Physical Sciences of the Ocean (IAPSO[3]) differs somewhat from that used in other fields. Table 1 summarizes the terms, units, and symbols for those quantities that have proven most useful in hydrologic optics. These quantities are defined and discussed in Secs. 42.3 to 43.5. Figure 1 summarizes the relationships among the various inherent and apparent optical properties. In the figure, note the central unifying role of radiative transfer theory. Note also that the spectral absorption coefficient and the spectral volume scattering function are the fundamental inherent optical properties in the sense that all inherent optical properties are derivable from those two. Likewise, spectral radiance is the parent of all radiometric quantities and apparent optical properties. The source term $S$ in the radiative transfer equation accounts both for true internal sources such as bioluminescence and for radiance appearing at the wavelength of interest owing to inelastic scattering from other wavelengths.

Most radiative transfer theory assumes the radiant energy to be monochromatic. In this case the associated optical properties and radiometric quantities are termed *spectral* and carry a wavelength ($\lambda$) argument or subscript (e.g., the spectral absorption coefficient $a(\lambda)$ or $a_\lambda$, or the spectral downward irradiance $E_d(\lambda)$). Spectral radiometric quantities have the SI unit $nm^{-1}$ added to the units shown in Table 1 (e.g., $E_d(\lambda)$ has units $W\,m^{-2}\,nm^{-1}$). Many radiometric instruments, on the other hand, respond to a fairly wide bandwidth, which complicates the comparison of data and theory.

**TABLE 1** Terms, Units, and Symbols for Quantities Commonly Used in Hydrologic Optics

| Quantity | SI units | IAPSO recommended symbol* | Historic symbol† (if different) |
|---|---|---|---|
| **Fundamental Quantities** | | | |
| Most of the fundamental quantities are not defined by IAPSO, in which case common usage is given. | | | |
| geometric depth below water surface | m | $z$ | |
| polar angle of photon travel | radian or degree | $\theta$ | |
| wavelength of light (in vacuo) | nm | $\lambda$ | |
| cosine of polar angle | dimensionless | $\mu \equiv \cos\theta$ | |
| optical depth below water surface | dimensionless | $\tau$ | |
| azimuthal angle of photon travel | radian or degree | $\phi$ | |
| scattering angle | radian or degree | $\psi$, $\gamma$ or $\Theta$ | $\theta$ |
| solid angle | sr | $\Omega$ or $\omega$ | $\Omega$ |
| **Radiometric Quantities** | | | |
| The quantities as shown represent broadband measurements. For narrowband (monochromatic) measurements add the adjective "spectral" to the term, add $nm^{-1}$ to the units, and add a wavelength index $\lambda$ to the symbol (e.g., spectral radiance, $L_\lambda$ or $L(\lambda)$) with units $W\,m^{-2}\,sr^{-1}\,nm^{-1}$. PAR is always broadband. | | | |
| (plane) irradiance | $W\,m^{-2}$ | $E$ | $H$ |
| downward irradiance | $W\,m^{-2}$ | $E_d$ | $H(-)$ |
| upward irradiance | $W\,m^{-2}$ | $E_u$ | $H(+)$ |
| net (vertical) irradiance | $W\,m^{-2}$ | $\bar{E}$ | $\bar{H}$ |
| scalar irradiance | $W\,m^{-2}$ | $E_o$ | $h$ |
| downward scalar irradiance | $W\,m^{-2}$ | $E_{od}$ | $h(-)$ |
| upward scalar irradiance | $W\,m^{-2}$ | $E_{ou}$ | $h(+)$ |
| radiant intensity | $W\,sr^{-1}$ | $I$ | $J$ |
| radiance | $W\,m^{-2}\,sr^{-1}$ | $L$ | $N$ |
| radiant excitance | $W\,m^{-2}$ | $M$ | $W$ |
| photosynthetically available radiation | photons $s^{-1}\,m^{-2}$ | PAR or $E_{PAR}$ | |
| quantity of radiant energy | J | $Q$ | $U$ |
| radiant power | W | $\Phi$ | $P$ |
| **Inherent Optical Properties** | | | |
| absorptance | dimensionless | $A$ | |
| absorption coefficient | $m^{-1}$ | $a$ | |
| scatterance | dimensionless | $B$ | |
| scattering coefficient | $m^{-1}$ | $b$ | $s$ |
| backward scattering coefficient | $m^{-1}$ | $b_b$ | $b$ |
| forward scattering coefficient | $m^{-1}$ | $b_f$ | $f$ |
| attenuance | dimensionless | $C$ | |
| attenuation coefficient | $m^{-1}$ | $c$ | $\alpha$ |
| (real) index of refraction | dimensionless | $n$ | |
| transmittance | dimensionless | $T$ | |
| volume scattering function | $m^{-1}\,sr^{-1}$ | $\beta$ | $\sigma$ |
| scattering phase function | $sr^{-1}$ | $\tilde{\beta}$ | $p$ |
| single-scattering albedo | dimensionless | $\omega_o$ or $\tilde{\omega}$ | |

**TABLE 1** Terms, Units, and Symbols for Quantities Commonly Used in Hydrological Optics (*Continued*)

| Quantity | SI units | IAPSO recommended symbol* | Historic symbol† (if different) |
|---|---|---|---|
| Apparent Optical Properties | | | |
| (vertical) attenuation coefficients: | | | |
| of downward irradiance $E_d(z)$ | $m^{-1}$ | $K_d$ | $K(-)$ |
| of total scalar irradiance $E_0(z)$ | $m^{-1}$ | $K_o$ | $k$ |
| of downward scalar irradiance $E_{0d}(z)$ | $m^{-1}$ | $K_{od}$ | $k(-)$ |
| of upward scalar irradiance $E_{0u}(z)$ | $m^{-1}$ | $K_{ou}$ | $k(+)$ |
| of PAR | $m^{-1}$ | $K_{PAR}$ | |
| of upward irradiance $E_u(z)$ | $m^{-1}$ | $K_u$ | $K(+)$ |
| of radiance $L(z, \theta, \phi)$ | $m^{-1}$ | $K(\theta, \phi)$ | |
| irradiance reflectance (ratio) | dimensionless | $R$ | $R(-)$ |
| average cosine of light field | dimensionless | $\bar{\mu}$ | |
| of downwelling light | dimensionless | $\bar{\mu}_d$ | $D(-) = 1/\bar{\mu}_d$ |
| of upwelling light | dimensionless | $\bar{\mu}_u$ | $D(+) = 1/\bar{\mu}_u$ |
| distribution function | dimensionless | | $D = 1/\bar{\mu}$ |

* References 1 and 3.
† Reference 2.

## 43.3 RADIOMETRIC QUANTITIES USEFUL IN HYDROLOGIC OPTICS

Consider an amount $\Delta Q$ of radiant energy incident in a time interval $\Delta t$ centered on time $t$, onto a surface of area $\Delta A$ located at $(x, y, z)$. The energy arrives through a set of directions contained in a solid angle $\Delta\Omega$ about the direction $(\theta, \phi)$ normal to the area $\Delta A$ and is produced by photons in a wavelength interval $\Delta\lambda$ centered on wavelength $\lambda$. Then an *operational* definition of the *spectral radiance* is

$$L(x, y, z, t, \theta, \phi, \lambda) \equiv \frac{\Delta Q}{\Delta t\, \Delta A\, \Delta\Omega\, \Delta\lambda} \qquad \mathrm{J\,s^{-1}\,m^{-2}\,sr^{-1}nm^{-1}}$$

In practice, one takes $\Delta t$, $\Delta A$, $\Delta\Omega$, and $\Delta\lambda$ small enough to get a useful resolution of radiance over the four parameter domains but not so small as to encounter diffraction effects or fluctuations from photon shot noise at very low light levels. Typical values are $\Delta t \sim 10^{-3}$ to $10^3$ s (depending on whether or not one wishes to average out sea surface wave effects), $\Delta A \sim 10^{-3}\,\mathrm{m}^2$, $\Delta\Omega \sim 10^{-2}$ sr, and $\Delta\lambda \sim 10$ nm. In the conceptual limit of infinitesimal parameter intervals, the spectral radiance is defined as

$$L(x, y, z, t, \theta, \phi, \lambda) \equiv \frac{\partial^4 Q}{\partial t\, \partial A\, \partial\Omega\, \partial\lambda} \qquad \mathrm{J\,s^{-1}\,m^{-2}\,sr^{-1}\,nm^{-1}}$$

Spectral radiance is the fundamental radiometric quantity of interest in hydrologic optics: it specifies the positional $(x, y, z)$, temporal $(t)$, directional $(\theta, \phi)$, and spectral $(\lambda)$ structure of the light field. For typical oceanic environments, horizontal variations (on a scale of tens to thousands of meters) of inherent and apparent optical properties are much less than variations with depth, and it is usually assumed that these properties vary only with depth $z$. Moreover, since the time scales for changes in IOPs or in the environment

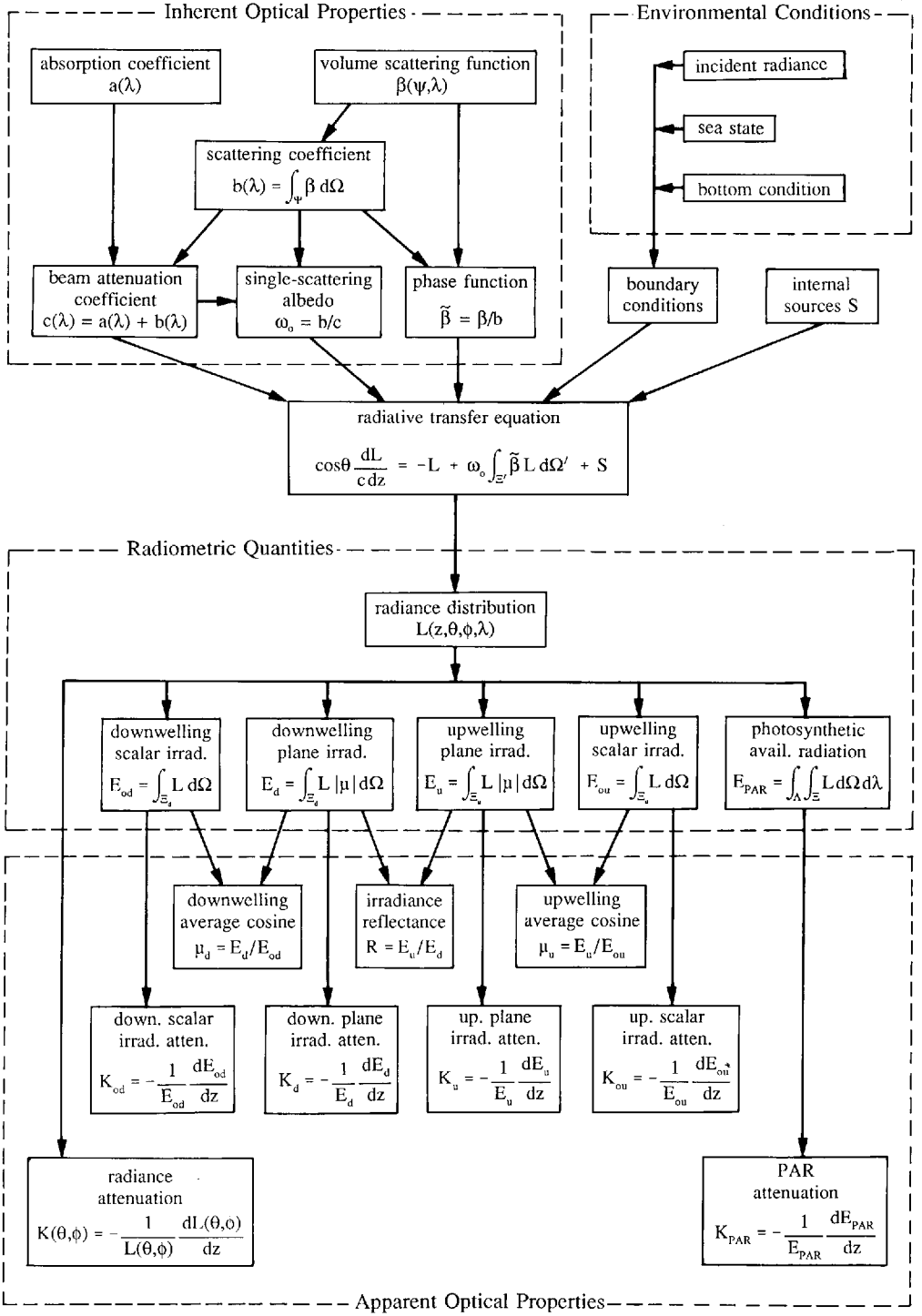


**FIGURE 1** Relationships between the various quantities commonly used in hydrologic optics.

(seconds to seasons) are much greater than the time required for the radiance field to reach steady state (microseconds) after a change in IOPs or boundary conditions, time-independent radiative transfer theory is adequate for most hydrologic optics studies. The spectral radiance therefore usually is written as $L(z, \theta, \phi, \lambda)$. The exceptions are applications such as time-of-flight lidar.

There are few conventions on the choice of coordinate systems. Oceanographers usually measure the depth $z$ positive downward from $z = 0$ at the mean water surface. In radiative transfer theory it is convenient to let $(\theta, \phi)$ denote the direction of photon travel (especially when doing Monte Carlo simulations). When displaying data it is convenient to let $(\theta, \phi)$ represent the direction in which the instrument was pointed (the viewing direction) in order to detect photons traveling in the opposite direction. Some authors measure the polar angle $\theta$ from the zenith (upward) direction, even when $z$ is taken as positive downward; others measure $\theta$ from the $+z$ axis (nadir, or downward, direction). In the following discussion $\Xi_u$ denotes the hemisphere of *upward* directions (i.e., the set of directions $(\theta, \phi)$ such that $0 \le \theta \le \pi/2$ and $0 \le \phi \le 2\pi$, *if* $\theta$ is measured from the zenith direction) and $\Xi_d$ denotes the hemisphere of *downward* directions. The element of solid angle is $d\Omega = \sin\theta\, d\theta\, d\phi$ with units of steradian. The solid angle measure of the set of directions $\Xi_u$ or $\Xi_d$ is $\Omega(\Xi_u) = \Omega(\Xi_d) = 2\pi$ sr.

Although the spectral radiance completely specifies the light field, it is seldom measured both because of instrumental difficulties and because such complete information often is not needed for specific applications. The most commonly measured radiometric quantities are various *irradiances.*

Consider a light detector constructed so as to be equally sensitive to photons of a given wavelength $\lambda$ traveling in any direction $(\theta, \phi)$ within a *hemisphere* of directions.[4] If the detector is located at depth $z$ and is oriented facing *upward,* so as to collect photons traveling *downward,* then the detector output is a measure of the *spectral downward scalar irradiance* at depth $z$, $E_{0d}(z, \lambda)$. Such an instrument is summing radiance over all the directions (elements of solid angle) in the downward hemisphere $\Xi_d$. Thus $E_{0d}(z, \lambda)$ is related to $L(z, \theta, \phi, \lambda)$ by

$$E_{0d}(z, \lambda) = \int_{\Xi_d} L(z, \theta, \phi, \lambda)\, d\Omega \qquad \mathrm{W\,m^{-2}\,nm^{-1}}$$

The symbolic integral over $\Xi_d$ can be evaluated as a double integral over $\theta$ and $\phi$ after a specific coordinate system is chosen.

If the same instrument is oriented facing *downward,* so as to detect photons traveling *upward,* then the quantity measured is the *spectral upward scalar irradiance* $E_{0u}(z, \lambda)$:

$$E_{0u}(z, \lambda) = \int_{\Xi_u} L(z, \theta, \phi, \lambda)\, d\Omega \qquad \mathrm{W\,m^{-2}\,nm^{-1}}$$

The *spectral scalar irradiance* $E_0(z, \lambda)$ is just the sum of the downward and upward components:

$$E_0(z, \lambda) \equiv E_{0d}(z, \lambda) + E_{0u}(z, \lambda) = \int_{\Xi} L(z, \theta, \phi, \lambda)\, d\Omega \qquad \mathrm{W\,m^{-2}\,nm^{-1}}$$

Here $\Xi = \Xi_d \cup \Xi_u$ is the set of all directions; $\Omega(\Xi) = 4\pi$ sr. $E_0(z, \lambda)$ is useful[2] because it is proportional to the spectral radiant energy density ($\mathrm{J\,m^{-3}\,nm^{-1}}$) at depth $z$.

Now consider a detector designed[4] so that its sensitivity is proportional to $|\cos\theta|$ where $\theta$ is the angle between the photon direction and the normal to the surface of the detector. This is the ideal response of a "flat plate" collector of area $\Delta A$, which when viewed at an angle $\theta$ to its normal appears to have an area of $\Delta A\,|\cos\theta|$. If such a detector is located at depth $z$ and is oriented facing *upward,* so as to detect photons traveling *downward,* then

its output is proportional to the *spectral downward plane irradiance* $E_d(z, \lambda)$ (usually called *spectral downwelling irradiance*). This instrument is summing the downwelling radiance weighted by the cosine of the photon direction:

$$E_d(z, \lambda) = \int_{\Xi_d} L(z, \theta, \phi, \lambda) |\cos \theta| \, d\Omega \qquad \text{W m}^{-2} \text{ nm}^{-1}$$

Turning this instrument upside down gives the *spectral upward plane irradiance* (*spectral upwelling irradiance*) $E_u(z, \lambda)$:

$$E_u(z, \lambda) = \int_{\Xi_u} L(z, \theta, \phi, \lambda) |\cos \theta| \, d\Omega \qquad \text{W m}^{-2} \text{ nm}^{-1}$$

$E_d$ and $E_u$ are useful because they give the energy flux (power per unit area) across the horizontal surface at depth $z$ owing to downwelling and upwelling photons, respectively.

The *spectral net irradiance* at depth $z$, $\bar{E}(z, \lambda)$, is the difference in the downwelling and upwelling plane irradiances:

$$\bar{E}(z, \lambda) = E_d(z, \lambda) - E_u(z, \lambda)$$

Photosynthesis is a quantum phenomenon (i.e., it is the *number* of available photons rather than the *amount* of radiant energy that is relevant to the chemical transformations). This is because if a photon of, say, $\lambda = 350$ nm, is absorbed by chlorophyll it induces the same chemical change as does a photon of $\lambda = 700$ nm, even though the 350-nm photon has twice the energy of the 700-nm photon. Only a part of the photon energy goes into photosynthesis; the excess is converted to heat or reradiated. Moreover, chlorophyll is equally able to absorb and utilize a photon regardless of the photon's direction of travel. Therefore, in studies of phytoplankton biology the relevant measure of the light field is the *photosynthetically available radiation,* PAR or $E_{PAR}$, defined by

$$\text{PAR}(z) \equiv \int_{350\,\text{nm}}^{700\,\text{nm}} \frac{\lambda}{hc} E_0(z, \lambda) \, d\lambda \qquad \text{photons s}^{-1} \text{ m}^{-2}$$

where $h = 6.6255 \times 10^{-34}$ J s is Planck's constant and $c = 3.0 \times 10^{17}$ nm s$^{-1}$ is the speed of light. The factor $\lambda/hc$ converts the energy units of $E_0$ (watts) to quantum units (photons per second). Bio-optical literature often states PAR values in units of mol photons s$^{-1}$ m$^{-2}$ or einst s$^{-1}$ m$^{-2}$. Morel and Smith[5] found that over a wide variety of water types from very clear to turbid, with corresponding variations in the spectral nature of the irradiance, the conversion factor for energy to quanta varied by only ±10 percent about the value $2.5 \times 10^{18}$ photons s$^{-1}$ W$^{-1}$ (4.2 μeinst s$^{-1}$ W$^{-1}$).

For practical reasons related to instrument design, PAR is sometimes estimated using the spectral downwelling plane irradiance and the visible wavelengths only:

$$\text{PAR}(z) \approx \int_{400\,\text{nm}}^{700\,\text{nm}} \frac{\lambda}{hc} E_d(z, \lambda) \, d\lambda \qquad \text{photons s}^{-1} \text{ m}^{-2}$$

However, it is now recognized[6,7] that the use of $E_d$ rather than $E_0$ can lead to errors of 20 to 100 percent in computations of PAR. Omission of the 350–400-nm band is less troublesome since those wavelengths are rapidly absorbed near the water surface, except in very clear waters.

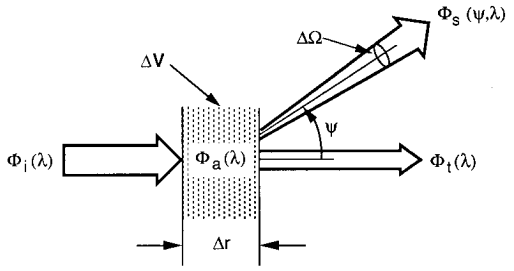


**FIGURE 2** Geometry used to define inherent optical properties.

## 43.4 INHERENT OPTICAL PROPERTIES

Consider a small volume $\Delta V$ of water of thickness $\Delta r$ as seen by a narrow collimated beam of monochromatic light of spectral radiant power $\Phi_i(\lambda)$ W nm$^{-1}$ as schematically illustrated in Fig. 2. Some part $\Phi_a(\lambda)$ of the incident power $\Phi_i(\lambda)$ is absorbed within the volume of water. Some part $\Phi_s(\psi, \lambda)$ is scattered out of the beam at an angle $\psi$, and the remaining power $\Phi_t(\lambda)$ is transmitted through the volume with no change in direction. Let $\Phi_s(\lambda)$ be the total power that is scattered into all directions. Furthermore, assume that no inelastic scattering occurs (i.e., assume that no photons undergo a change in wavelength during the scattering process). Then by conservation of energy,

$$\Phi_i(\lambda) = \Phi_a(\lambda) + \Phi_s(\lambda) + \Phi_t(\lambda)$$

The *spectral absorptance* $A(\lambda)$ is the fraction of incident power that is absorbed within the volume:

$$A(\lambda) \equiv \frac{\Phi_a(\lambda)}{\Phi_i(\lambda)}$$

Likewise the *spectral scatterance* $B(\lambda)$ is the fractional part of the incident power that is scattered out of the beam,

$$B(\lambda) \equiv \frac{\Phi_s(\lambda)}{\Phi_i(\lambda)}$$

and the *spectral transmittance* $T(\lambda)$ is

$$T(\lambda) \equiv \frac{\Phi_t(\lambda)}{\Phi_i(\lambda)}$$

Clearly, $A(\lambda) + B(\lambda) + T(\lambda) = 1$. A quantity easily confused with the absorptance $A(\lambda)$ is the *absorbance* $D(\lambda)$ (also called *optical density*) defined as[8]

$$D(\lambda) \equiv \log_{10} \frac{\Phi_i(\lambda)}{\Phi_s(\lambda) + \Phi_t(\lambda)} = -\log_{10} [1 - A(\lambda)]$$

$D(\lambda)$ is the quantity actually measured in a spectrophotometer.

The inherent optical properties usually employed in hydrologic optics are the spectral absorption and scattering coefficients which are, respectively, the spectral absorptance and

scatterance *per unit distance* in the medium. In the geometry of Fig. 2, the *spectral absorption coefficient* $a(\lambda)$ is defined as

$$a(\lambda) \equiv \lim_{\Delta r \to 0} \frac{A(\lambda)}{\Delta r} \qquad \mathrm{m}^{-1}$$

and the *spectral scattering coefficient* $b(\lambda)$ is

$$b(\lambda) \equiv \lim_{\Delta r \to 0} \frac{B(\lambda)}{\Delta r} \qquad \mathrm{m}^{-1}$$

The *spectral beam attenuation coefficient* $c(\lambda)$ is defined as

$$c(\lambda) \equiv a(\lambda) + b(\lambda)$$

Hydrologic optics uses the term attenuation rather than extinction.

Now take into account the angular distribution of the scattered power, with $B(\psi, \lambda)$ being the fraction of incident power scattered out of the beam through an angle $\psi$ into a solid angle $\Delta\Omega$ centered on $\psi$ as shown in Fig. 2. Then the angular scatterance per unit distance and unit solid angle, $\beta(\psi, \lambda)$, is

$$\beta(\psi, \lambda) \equiv \lim_{\Delta r \to 0} \lim_{\Delta\Omega \to 0} \frac{B(\psi, \lambda)}{\Delta r\, \Delta\Omega} = \lim_{\Delta r \to 0} \lim_{\Delta\Omega \to 0} \frac{\Phi_s(\psi, \lambda)}{\Phi_i(\lambda)\, \Delta r\, \Delta\Omega} \qquad \mathrm{m}^{-1}\,\mathrm{sr}^{-1}$$

The spectral power scattered into the given solid angle $\Delta\Omega$ is just the spectral radiant intensity scattered into direction $\psi$ times the solid angle: $\Phi_s(\psi, \lambda) = I_s(\psi, \lambda)\, \Delta\Omega$. Moreover, if the incident power $\Phi_i(\lambda)$ falls on an area $\Delta A$, then the corresponding incident irradiance is $E_i(\lambda) = \Phi_i(\lambda)/\Delta A$. Noting that $\Delta V = \Delta r\, \Delta A$ is the volume of water that is illuminated by the incident beam gives

$$\beta(\psi, \lambda) = \lim_{\Delta V \to 0} \frac{I_s(\psi, \lambda)}{E_i(\lambda)\, \Delta V}$$

This form of $\beta(\psi, \lambda)$ suggests the name *spectral volume scattering function* and the physical interpretation of scattered intensity per unit incident irradiance per unit volume of water; $\beta(\psi, \lambda)$ also can be interpreted as the differential scattering cross section per unit volume. Integrating $\beta(\psi, \lambda)$ over all directions (solid angles) gives the total scattered power per unit incident irradiance and unit volume of water or, in other words, the spectral scattering coefficient:

$$b(\lambda) = \int_{\Xi} \beta(\psi, \lambda)\, d\Omega = 2\pi \int_0^{\pi} \beta(\psi, \lambda) \sin\psi\, d\psi$$

The last equation follows because scattering in natural waters is azimuthally symmetric about the incident direction (for unpolarized sources and for randomly oriented scatterers). This integration is often divided into forward scattering, $0 \le \psi \le \pi/2$, and backward scattering, $\pi/2 \le \psi \le \pi$, parts. The corresponding spectral forward and backward scattering coefficients are, respectively,

$$b_f(\lambda) \equiv 2\pi \int_0^{\pi/2} \beta(\psi, \lambda) \sin\psi\, d\psi$$

$$b_b(\lambda) \equiv 2\pi \int_{\pi/2}^{\pi} \beta(\psi, \lambda) \sin\psi\, d\psi$$

The preceding discussion has assumed that no inelastic (transpectral) scattering processes are present. However, transpectral scattering does occur in natural waters

attributable to fluorescence by dissolved matter or chlorophyll and to Raman or Brillouin scattering by the water molecules themselves (see Sec. 43.23). Power lost from wavelength $\lambda$ by scattering into wavelength $\lambda' \neq \lambda$ appears in the above formalism as an increase in the spectral absorption.[9] In this case, $a(\lambda)$ accounts for "true" absorption (e.g., conversion of radiant energy into heat) as well as for the loss of power at wavelength $\lambda$ by inelastic scattering to another wavelength. The gain in power at $\lambda'$ appears as a source term in the radiative transfer formalism.

Two more inherent optical properties are commonly used in hydrologic optics. The *spectral single-scattering albedo* $\omega_0(\lambda)$ is

$$\omega_0(\lambda) \equiv \frac{b(\lambda)}{c(\lambda)}$$

The single-scattering albedo is the probability that a photon will be scattered (rather than absorbed) in any given interaction; hence, $\omega_0(\lambda)$ is also known as the *probability of photon survival.* The *spectral volume scattering phase function,* $\tilde{\beta}(\psi, \lambda)$, is defined by

$$\tilde{\beta}(\psi, \lambda) \equiv \frac{\beta(\psi, \lambda)}{b(\lambda)} \qquad \text{sr}^{-1}$$

Writing the volume scattering function $\beta(\psi, \lambda)$ as the product of the scattering coefficient $b(\lambda)$ and the phase function $\tilde{\beta}(\psi, \lambda)$ partitions $\beta(\psi, \lambda)$ into a factor giving the *strength* of the scattering, $b(\lambda)$ with units of $\text{m}^{-1}$, and a factor giving the *angular distribution* of the scattered photons, $\tilde{\beta}(\psi, \lambda)$ with units of $\text{sr}^{-1}$.

## 43.5 APPARENT OPTICAL PROPERTIES

The quantity

$$\bar{\mu}_\text{d}(z, \lambda) \equiv \frac{\displaystyle\int_{\Xi_\text{d}} L(z, \theta, \phi, \lambda) |\cos\theta| \, d\Omega}{\displaystyle\int_{\Xi_\text{u}} L(z, \theta, \phi, \lambda) \, d\Omega} \equiv \frac{E_\text{d}(z, \lambda)}{E_{0\text{d}}(z, \lambda)}$$

is called the *spectral downwelling average cosine.* The definition shows that $\bar{\mu}_\text{d}(z, \lambda)$ is the average value of the cosine of the polar angle of all the photons contributing to the downwelling radiance at the given depth and wavelength. The *spectral upwelling average cosine* is defined analogously:

$$\bar{\mu}_\text{u}(z, \lambda) \equiv \frac{E_\text{u}(z, \lambda)}{E_{0\text{u}}(z, \lambda)}$$

The average cosines are useful one-parameter measures of the directional structures of the downwelling and upwelling light fields. For example, if the downwelling light field (radiance distribution) is collimated in direction $(\theta_0, \phi_0)$ so that $L(\theta, \phi) = L_0\delta(\theta - \theta_0)\delta(\phi - \phi_0)$, where $\delta$ is the Dirac $\delta$ function, then $\bar{\mu}_\text{d} = |\cos\theta_0|$. If the downwelling radiance is completely diffuse (isotropic), $L(\theta, \phi) = L_0$ and $\bar{\mu}_\text{d} = \frac{1}{2}$. Typical values of the average cosines for waters illuminated by the sun and sky are $\bar{\mu}_\text{d} \approx \frac{3}{4}$ and $\bar{\mu}_\text{u} \approx \frac{3}{8}$. Older literature generally refers to *distribution functions,* $D_\text{d}$ and $D_\text{u}$, rather than to average cosines. The distribution functions are just reciprocals of the average cosines:

$$D_\text{d}(z, \lambda) = \frac{1}{\bar{\mu}_\text{d}(z, \lambda)} \qquad \text{and} \qquad D_\text{u}(z, \lambda) = \frac{1}{\bar{\mu}_\text{u}(z, \lambda)}$$

The *spectral irradiance reflectance* (or *irradiance ratio*) $R(z, \lambda)$ is the ratio of spectral upwelling to downwelling plane irradiances:

$$R(z, \lambda) \equiv \frac{E_u(z, \lambda)}{E_d(z, \lambda)}$$

$R(z, \lambda)$ just beneath the sea surface is of great importance in remote sensing (see Sec. 43.22).

Under typical oceanic conditions for which the incident lighting is provided by the sun and sky, the various radiances and irradiances all decrease approximately exponentially with depth, at least when far enough below the surface (and far enough above the bottom, in shallow water) to be free of boundary effects. For example, it is convenient to write the depth dependence of $E_d(z, \lambda)$ as

$$E_d(z, \lambda) \equiv E_d(0, \lambda) \exp\left[-\int_0^z K_d(z', \lambda)\, dz'\right] \equiv E_d(0, \lambda) \exp\left[-\bar{K}_d(\lambda) z\right]$$

where $K_d(z, \lambda)$ is the *spectral diffuse attenuation coefficient* for spectral downwelling plane irradiance and $\bar{K}_d(\lambda)$ is the average value of $K_d(z, \lambda)$ over the depth interval 0 to $z$. Solving for $K_d(z, \lambda)$ gives

$$K_d(z, \lambda) = -\frac{d \ln E_d(z, \lambda)}{dz} = -\frac{1}{E_d(z, \lambda)} \frac{dE_d(z, \lambda)}{dz} \qquad \text{m}^{-1}$$

The distinction between *beam* and *diffuse* attenuation coefficients is important. The beam attenuation coefficient $c(\lambda)$ is defined in terms of the radiant power lost from a single, narrow, collimated beam of photons. The downwelling diffuse attenuation coefficient $K_d(z, \lambda)$ is defined in terms of the decrease with depth of the ambient downwelling irradiance $E_d(z, \lambda)$, which comprises photons heading in all downward directions (a diffuse or uncollimated light field). $K_d(z, \lambda)$ clearly depends on the directional structure of the ambient light field and so is classified as an apparent optical property. Other diffuse attenuation coefficients, e.g., $K_u$, $K_{od}$, $K_{ou}$, $K_{PAR}$, and $K(\theta, \phi)$, are defined in an analogous manner, using the corresponding radiometric quantities.

In *homogeneous* waters, these "$K$ functions" depend only weakly on depth and therefore can serve as convenient, if imperfect, descriptors of the water body. Smith and Baker[10] have pointed out other reasons why $K$ functions are useful:

1. The $K$'s are defined as ratios and therefore do not require absolute radiometric measurements.
2. The $K$'s are strongly correlated with chlorophyll concentration (i.e., they provide a connection between biology and optics).
3. About 90 percent of the diffusely reflected light from a water body comes from a layer of water of depth $1/K_d(0, \lambda)$ (i.e., $K_d$ has implications for remote sensing).
4. Radiative transfer theory provides several useful relations between the $K$'s and other quantities of interest, such as absorption and beam attenuation coefficients, the irradiance reflectance, and the average cosines.
5. Instruments are available for routine measurement of the $K$'s.

It must be remembered, however, that in spite of their utility $K$ functions are apparent optical properties—a change in the environment (e.g., solar angle or sea state) changes their value, sometimes by a negligible amount but sometimes greatly. However, numerical simulations by Gordon[11] show how with a few additional but easily made measurements measured values of $K_d(z, \lambda)$ and $\bar{K}_d(\lambda)$ can be "normalized" to remove the effects of solar angle and sea state. The normalized $K_d$ and $\bar{K}_d$ are equal to the values that would be

obtained if the sun were at the zenith and the sea surface were calm. *If* this normalization is performed, the resulting $K_d(z, \lambda)$ and $\bar{K}_d(\lambda)$ can be regarded as *inherent* optical properties for all practical purposes. It is strongly recommended that Gordon's procedure be routinely followed by experimentalists.

## 43.6 THE OPTICALLY SIGNIFICANT CONSTITUENTS OF NATURAL WATERS

### Dissolved Substances

Pure sea water consists of pure water plus various dissolved salts, which average about 35 parts per thousand (‰) by weight. These salts increase scattering above that of pure water by 30 percent (see Table 10 in Sec. 43.17). It is not well established what, if any, effect these salts have on absorption, but it is likely that they increase absorption somewhat at ultraviolet wavelengths.

Both fresh and saline waters contain varying concentrations of dissolved organic compounds. These compounds are produced during the decay of plant matter and consist mostly of various humic and fulvic acids.[8] These compounds are generally brown in color and in sufficient concentrations can color the water yellowish brown. For this reason the compounds are generically referred to as *yellow matter, Gelbstoff,* or *gilvin.* Yellow matter absorbs very little in the red, but absorption increases rapidly with decreasing wavelength. Since the main source of yellow matter is decayed terrestrial vegetation, concentrations are generally greatest in lakes, rivers, and coastal waters influenced by river runoff. In such waters yellow matter can be the dominant absorber at the blue end of the spectrum. In mid-ocean waters absorption by yellow matter is usually small compared to absorption by other constituents, but some yellow matter is likely to be present as the result of decaying phytoplankton, especially at the end of a bloom.

### Particulate Matter

Particulate matter in the oceans has two distinct origins: biological and physical. The organic particles of optical importance are created as bacteria, phytoplankton, and zooplankton grow and reproduce by photosynthesis or by eating their neighbors. Particles of a given size are destroyed by breaking apart after death, by flocculation into larger aggregate particles, or by settling out of the water column. Inorganic particles are created primarily by weathering of terrestrial rocks and soils. These particles can enter the water as wind-blown dust settles on the sea surface, as rivers carry eroded soil to the sea, or as currents resuspend bottom sediments. Inorganic particles are removed from the water by settling, aggregating, or dissolving. This particulate matter usually is the major determiner of both the absorption and scattering properties of natural waters and is responsible for most of the temporal and spatial variability in these optical properties.

***Organic Particles.*** These occur in many forms.

*Viruses.* Natural marine waters contain virus particles[12] in concentrations of $10^{12}$ to $10^{15}$ particles $m^{-3}$. These particles are generally much smaller (2–200 nm) than the wavelength of visible light, and it is not known what, if any, direct effect viruses have on the optical properties of sea water.

*Colloids.* Nonliving collodial particles in the size range 0.4–1.0 μm are found[13] in typical number concentrations of $10^{13}\,m^{-3}$ and colloids of size $\leq 0.1$ μm are found[14] in abundances of $10^{15}\,m^{-3}$. Some of the absorption traditionally attributed to dissolved matter may be due to colloids, some of which strongly resemble fulvic acids in electron micrographs.[14]

*Bacteria.* Living bacteria in the size range 0.2–1.0 μm occur in typical number concentrations of $10^{11}$–$10^{13}$ $m^{-3}$. It only recently has been recognized[15–17] that bacteria can be significant scatterers and absorbers of light, expecially at blue wavelengths and in clean oceanic waters where the larger phytoplankton are relatively scarce.

*Phytoplankton.* These ubiquitous microscopic plants occur with incredible diversity of species, size, shape, and concentration. They range in cell size from less than 1 μm to more than 200 μm, and some species form even larger chains of individual cells. It has long been recognized that phytoplankton are the particles primarily responsible for determining the optical properties of most oceanic waters. Their chlorophyll and related pigments strongly absorb light in the blue and red and thus when concentrations are high determine the spectral absorption of sea water. These particles are generally much larger than the wavelength of visible light and are efficient scatterers, especially via diffraction, thus influencing the scattering properties of sea water.

*Organic Detritus.* Nonliving organic particles of various sizes are produced, for example, when phytoplankton die and their cells break apart. They may also be formed when zooplankton graze on phytoplankton and leave behind cell fragments and fecal pellets. Even if these detrital particles contain pigments at the time of their production, they can be rapidly photo-oxidized and lose the characteristic absorption spectrum of living phytoplankton, leaving significant absorption only at blue wavelengths.

*Large Particles.* Particles larger than 100 μm include zooplankton (living animals with sizes from tens of micrometers to two centimeters) and fragile amorphous aggregates[18] of smaller particles ("marine snow," with sizes from 0.5 mm to tens of centimeters). Such particles occur in highly variable numbers from almost none to thousands per cubic meter. Even at relatively large concentrations these large particles tend to be missed by optical instruments that randomly sample only a few cubic centimeters of water or that mechanically break apart the aggregates. However, these large particles can be efficient diffuse scatterers of light and therefore may significantly affect the optical properties (especially backscatter) of large volumes of water, e.g., as seen by remote sensing instruments. Although such optical effects are recognized, they have not been quantified.

***Inorganic Particles.*** These generally consist of finely ground quartz sand, clay minerals, or metal oxides in the size range from much less than 1 μm to several tens of micrometers. Insufficient attention has been paid to the optical effects of such particles in sea water, although it is recognized that inorganic particles are sometimes optically more important than organic particles. Such situations can occur both in turbid coastal waters carrying a heavy sediment load and in very clear oceanic waters which are receiving wind-blown dust.[19]

At certain stages of its life, the phytoplankton coccolithophore species *Emiliania huxleyi* is a most remarkable source of crystalline particles. During blooms *E. huxleyi* produces and sheds enormous numbers of small (2–4 μm) calcite plates; concentrations of $3 \times 10^{11}$ plates $m^{-3}$ have been observed.[20] Although they have a negligible effect on light absorption, these calcite plates are extremely efficient light scatterers: irradiance reflectances of $R = 0.39$ have been observed[20] at blue wavelengths during blooms (compared with $R = 0.02$ to 0.05 in the blue for typical ocean waters, discussed in Sec. 43.22). Such coccolithophore blooms give the ocean a milky white or turquoise appearance.

## 43.7 PARTICLE SIZE DISTRIBUTIONS

In spite of the diverse mechanisms for particle production and removal, observation shows that a single family of particle size distributions often suffices to describe oceanic particulate matter in the optically important size range from 0.1 to 100 μm. Let $N(x)$ be

the number of particles per unit volume with size greater than $x$ in a sample of particles; $x$ usually represents equivalent spherical diameter computed from particle volume, but also can represent particle volume or surface area. The Junge (also called *hyperbolic*) cumulative size distribution[21] is then

$$N(x) = k\left(\frac{x}{x_0}\right)^{-m}$$

where $k$ sets the scale, $x_0$ is a reference size, and $-m$ is the slope of the distribution when $\log N$ is plotted versus $\log x$; $k$, $x_0$, and $m$ are positive constants.

Oceanic particle size distributions usually have $m$ values between 2 and 5, with $m = 3$ to 4 being typical; such spectra can be seen in McCave,[22] fig. 7. It often occurs that oceanic particle size spectra are best described by a segmented distribution in which a smaller value of $m$ is used for $x$ less than a certain value and a larger value of $m$ is used for $x$ greater than that value. Such segmented spectra can be seen in Bader,[21] and in McCave,[22] fig. 8.

The quantity most relevant to optics, e.g., in Mie scattering computations for polydisperse systems, is not the *cumulative* size distribution $N(x)$, but rather the *number* size distribution $n(x)$. The number distribution is defined such that $n(x)\,dx$ is the number of particles in the size interval from $x$ to $x + dx$. The number distribution is related to the cumulative distribution by $n(x) = |dN(x)/dx|$, so that for the Junge distribution

$$n(x) = kmx_0^{-m}x^{-m-1} \equiv Kx^{-s}$$

where $K \equiv kmx_0^{-m}$ and $s \equiv m + 1$; $s$ is commonly referred to as the slope of the distribution. Figure 3 shows the number distribution of biological particles typical of open ocean waters; note that a value of $s = 4$ gives a reasonable fit to the plotted points.

It should be noted, however, that the Junge distribution sometimes fails to represent

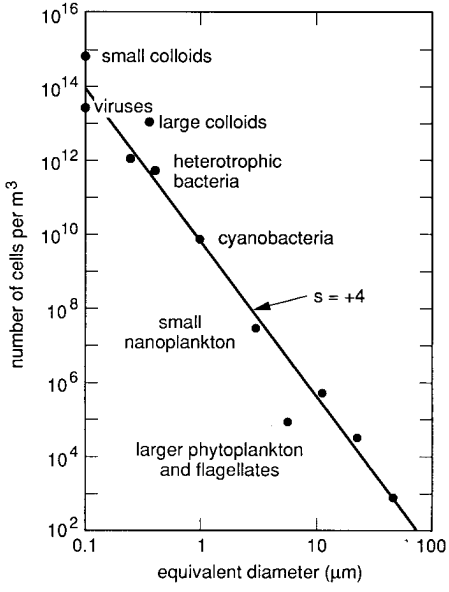


**FIGURE 3** Number size distribution typical of biological particles in the open ocean. (*Based on Stramski and Kiefer,*[17] *with permission.*)

oceanic conditions. For example, during the growth phase of a phytoplankton bloom the rapid increase in population of a particular species may give abnormally large numbers of particles in a particular size range. Such bloom conditions therefore give a "bump" in $n(x)$ that is not well modeled by the simple Junge distribution. Moreover, Lambert et al.[23] found that a log-normal distribution sometimes better described the distributions of inorganic particles found in water samples taken from near the bottom at deep ocean locations. These particles were principally aluminosilicates in the 0.2–10.0-μm size range but included quartz grains, metal oxides, and phytoplankton skeletal parts such as coccolithophore plates. Based on the sampling location it was assumed that the inorganic particles were resuspended sediments. Lambert et al. found that the size distributions of the individual particle types (e.g., aluminosilicates or metal oxides) obeyed log-normal distributions which "flattened out" below 1 μm. For particles larger than ~1 μm, log-normal and Junge distributions gave nearly equivalent descriptions of the data. Biological particles were not as well described by the log-normal distribution, especially for sizes greater than 5 μm.

## 43.8 ELECTROMAGNETIC PROPERTIES OF WATER

In studies of electromagnetic wave propagation at the level of Maxwell's equations it is convenient to specify the bulk electromagnetic properties of the medium via the electrical permittivity $\varepsilon$, the magnetic permeability $\mu$, and the elecrical conductivity $\sigma$. Since water displays no significant magnetic properties, the permeability can be taken equal to the free-space (in vacuo) value at all frequencies: $\mu = \mu_0 = 4\pi \times 10^{-7}\,\mathrm{N\,A^{-2}}$. Both $\varepsilon$ and $\sigma$ depend on the frequency $\omega$ of the propagating electromagnetic wave as well as on the water temperature, pressure, and salinity. Low-frequency ($\omega \to 0$) values for the permittivity are of order $\varepsilon \approx 80\varepsilon_0$, where $\varepsilon_0 = 8.85 \times 10^{-12}\,\mathrm{A^2\,s^2\,N^{-1}\,m^{-2}}$ is the free-space value. This value decreases to $\varepsilon \approx 1.8\varepsilon_0$ at optical frequencies. Extensive tabulations of $\varepsilon/\varepsilon_0$ as a function of temperature and pressure are given for pure water in Archer and Wang.[24] The low-frequency conductivity ranges from $\sigma \approx 4 \times 10^{-6}$ siemen $\mathrm{m^{-1}}$ for pure water to $\sigma \approx 4.4$ siemen $\mathrm{m^{-1}}$ for sea water.

The effects of $\varepsilon$, $\mu$, and $\sigma$ on electromagnetic wave propagation are compactly summarized in terms of the complex index of refraction, $m = n - \mathrm{i}k$, where $n$ is the real index of refraction, $k$ is the dimensionless electrodynamic absorption coefficient, and $\mathrm{i} = \sqrt{(-1)}$; $n$ and $k$ are collectively called the *optical constants* of water (a time dependence convention of $\exp(+\mathrm{i}\omega t)$ is used in deriving wave equations from Maxwell's equations). The explicit dependence of $m$ on $\varepsilon$, $\mu$, and $\sigma$ is given by[25]

$$m^2 = \mu\varepsilon c^2 - i\frac{\mu\sigma c^2}{\omega}$$

$$= (n - \mathrm{i}k)^2 = n^2 - k^2 - \mathrm{i}2nk$$

where $c = (\varepsilon_0\mu_0)^{-1/2}$ is the speed of light in vacuo. These equations can be used to relate $n$ and $k$ to the bulk electromagnetic properties. The optical constants are convenient because they are directly related to the scattering and absorbing properties of water. The real index of refraction $n(\lambda)$ governs scattering both at interfaces (via the laws of reflection and refraction) and within the medium (via thermal or other fluctuations of $n(\lambda)$ at molecular and larger scales). The spectral absorption coefficient $a(\lambda)$ is related to $k(\lambda)$ by[25]

$$a(\lambda) = \frac{4\pi k(\lambda)}{\lambda}$$

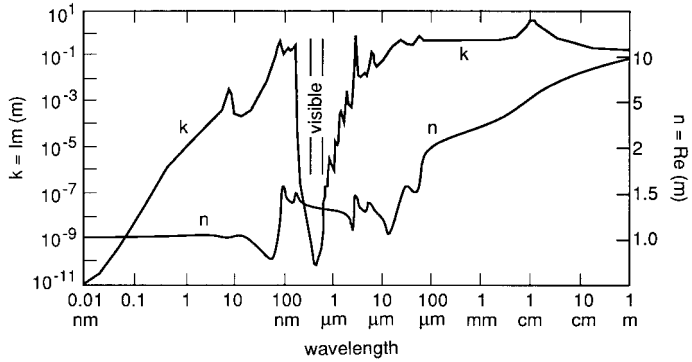


**FIGURE 4** The optical constants of pure water. The left axis gives $k = \mathrm{Im}(m)$ and the right axis gives $n = \mathrm{Re}(m)$ where $m$ is the complex index of refraction. (*Redrawn from Zoloratev and Demin,*[26] *with permission.*)

Here $\lambda$ refers to the in vacuo wavelength of light corresponding to a given frequency $\omega$ of electromagnetic wave.

Figure 4 shows the wavelength dependence of the optical constants $n$ and $k$ for pure water. The extraordinary feature seen in this figure is the narrow "window" in $k(\lambda)$, where $k(\lambda)$ decreases by over nine orders of magnitude between the near ultraviolet and the visible and then quickly rises again in the near infrared. This behavior in $k(\lambda)$ gives a corresponding window in the spectral absorption coefficient $a(\lambda)$ as seen in Table 2. Because of the opaqueness of water outside the near-UV to near-IR wavelengths, hydrologic optics is concerned with only this small part of the electromagnetic spectrum. These wavelengths overlap nicely with the wavelengths of the sun's maximum energy output and with a corresponding window in atmospheric absorption, much to the benefit of life on earth.

## 43.9 INDEX OF REFRACTION

### Seawater

Austin and Halikas[27] exhaustively reviewed the literature on measurements of the real index of refraction of sea water. Their report contains extensive tables and interpolation algorithms for the index of refraction (relative to air), $n(\lambda, S, T, p)$, as a function of wavelength ($\lambda = 400$–$700$ nm), salinity ($S = 0$–$43$‰), temperature ($T = 0$–$30$°C), and pressure ($p = 10^5$–$10^8$ Pa, or 1 to 1080 atm). Figure 5 illustrates the general dependence of $n$ on these four parameters: $n$ decreases with increasing wavelength or temperature and increases with increasing salinity or pressure. Table 3 gives the values of $n$ for the extreme values of each parameter. The extreme values of $n$, 1.329128 and 1.366885, show that $n$ varies by less than 3 percent over the entire parameter range relevant to hydrologic optics. Table 4 gives selected values of $n(\lambda, T)$ for fresh water ($S = 0$) and for typical sea water ($S = 35$‰) at atmospheric pressure ($p = 10^5$ Pa). The values in Table 4 can be multiplied by 1.000293 (the index of refraction of dry air at STP and $\lambda = 538$ nm) if values relative to vacuum are desired. Millard and Seaver[28] have developed a 27-term formula that gives the

**TABLE 2** Absorption Coefficient $a$ of Pure Water As a Function of Wavelength $\lambda$*

| $\lambda$ | $a$ ($m^{-1}$) | $\lambda$ | $a$ ($m^{-1}$) |
|---|---|---|---|
| 0.01 nm | $1.3 \times 10^{1}$ | 700 nm | 0.650 |
| 0.1 | $6.5 \times 10^{2}$ | 800 | 2.07 |
| 1 | $9.4 \times 10^{4}$ | 900 nm | 7.0 |
| 10 | $3.5 \times 10^{6}$ | 1 μm | $3.3 \times 10^{1}$ |
| 100 | $5.0 \times 10^{7}$ | 10 | $7.0 \times 10^{4}$ |
| 200 | 3.07 | 100 μm | $6.5 \times 10^{4}$ |
| 300 | 0.141 | 0.001 m | $1.3 \times 10^{4}$ |
| 400 | 0.0171 | 0.01 | $3.6 \times 10^{3}$ |
| 500 | 0.0257 | 0.1 | $5.0 \times 10^{1}$ |
| 600 nm | 0.244 | 1 m | 2.5 |

* Data for $200\,\text{nm} \leq \lambda \leq 800\,\text{nm}$ taken from Table 6. Data for other wavelengths computed from Fig. 4.

index of refraction to part-per-million accuracy over most of the oceanographic parameter range.

## Particles

Suspended particulate matter in sea water often has a bimodal index of refraction distribution. Living phytoplankton typically have "low" indices of refraction in the range 1.01 to 1.09 relative to the index of refraction of seawater. Detritus and inorganic particles generally have "high" indices in the range of 1.15 to 1.20 relative to seawater.[29] Typical values are 1.05 for phytoplankton and 1.16 for inorganic particles.

Table 5 gives the relative index of refraction of terrigenous minerals commonly found in river runoff and wind-blown dust. Only recently has it become possible to measure the refractive indices of individual phytoplankton cells.[30] Consequently, little is yet known

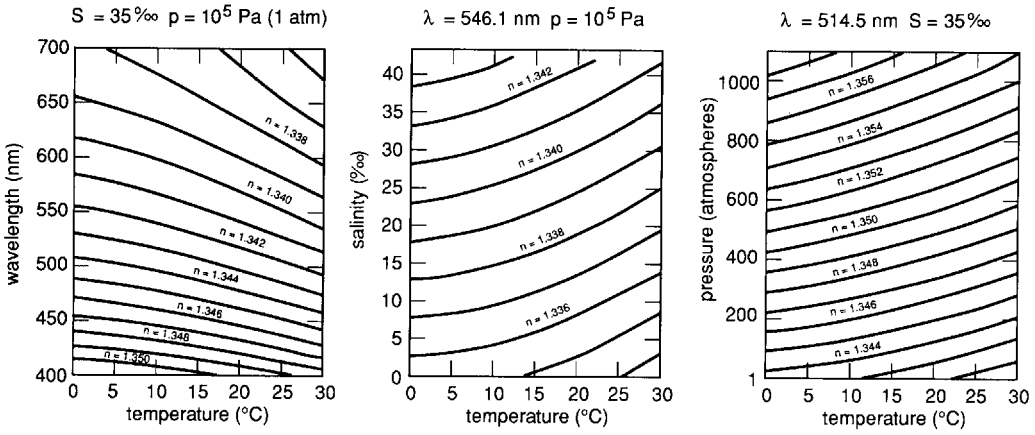


**FIGURE 5** Real index of refraction of water for selected values of pressure, temperature, and salinity. (*Adapted from Austin and Halikas.*[27])

**TABLE 3** Index of Refraction of Water $n$ for the Extreme Values of Pressure $p$, Temperature $T$, Salinity $S$, and Wavelength $\lambda$ Encountered in Hydrologic Optics*

| $p$ (Pa) | $T$ (°C) | $S$ (‰) | $\lambda$ (nm) | $n$ |
|---|---|---|---|---|
| $1.01 \times 10^5$ | 0 | 0 | 400 | 1.344186 |
| 1.01 | 0 | 0 | 700 | 1.331084 |
| 1.01 | 0 | 35 | 400 | 1.351415 |
| 1.01 | 0 | 35 | 700 | 1.337906 |
| 1.01 | 30 | 0 | 400 | 1.342081 |
| 1.01 | 30 | 0 | 700 | 1.329128 |
| 1.01 | 30 | 35 | 400 | 1.348752 |
| 1.01 | 30 | 35 | 700 | 1.335316 |
| $1.08 \times 10^8$ | 0 | 0 | 400 | 1.360076 |
| 1.08 | 0 | 0 | 700 | 1.346604 |
| 1.08 | 0 | 35 | 400 | 1.366885 |
| 1.08 | 0 | 35 | 700 | 1.352956 |
| 1.08 | 30 | 0 | 400 | 1.356281 |
| 1.08 | 30 | 0 | 700 | 1.342958 |
| 1.08 | 30 | 35 | 400 | 1.362842 |
| 1.08 | 30 | 35 | 700 | 1.348986 |

* Reproduced from Austin and Halikas.[27]

about the dependence of refractive index on phytoplankton species, or on the physiological state of the plankton within a given species, although it appears that the dependence can be significant.[31]

## 43.10 MEASUREMENT OF ABSORPTION

Determination of the spectral absorption coefficient $a(\lambda)$ for natural waters is a difficult task for several reasons. First, water absorbs only weakly at near-UV to blue wavelengths so that very sensitive instruments are required. More importantly, scattering is never negligible so that careful consideration must be made of the possible aliasing of the absorption measurements by scattering effects. In pure water at wavelengths of $\lambda = 370$ to 450 nm, molecular scattering provides 20 to 25 percent (Table 10) of the total beam attenuation, $c(\lambda) = a(\lambda) + b(\lambda)$. Scattering effects can dominate absorption at all visible wavelengths in waters with high particulate loads. Additional complications arise in determining the absorption of pure water because of the difficulty of preparing uncontaminated samples.

Many techniques have been employed in attempts to determine the spectral absorption coefficient for pure water, $a_w(\lambda)$; these are reviewed in Smith and Baker.[32] The most commonly employed technique for routine determination of $a(\lambda)$ for oceanic waters consists of filtering a sample of water to retain the particulate matter on a filter pad. The spectral absorption of the particulate matter, $a_p(\lambda)$, is then determined in a spectrophotometer. The absorption of pure water, $a_w(\lambda)$, must be added to $a_p(\lambda)$ to obtain the total absorption of the oceanic water sample. Even though this technique for determining absorption has been in use for many years, the methodology is still evolving[33–35] because of the many types of errors inherent in the $a_p(\lambda)$ measurements (e.g., inability of filters to

**TABLE 4** Index of Refraction of Fresh Water and of Sea Water at Atmospheric Pressure for Selected Temperatures and Wavelengths*

| | Fresh Water ($S = 0$) Wavelength (nm) | | | | | | | |
|---|---|---|---|---|---|---|---|---|
| Temp (°C) | 400 | 420 | 440 | 460 | 480 | 500 | 520 | 540 |
| 0 | 1.34419 | 1.34243 | 1.34092 | 1.33960 | 1.33844 | 1.33741 | 1.33649 | 1.33567 |
| 10 | 1.34390 | 1.34215 | 1.34064 | 1.33933 | 1.33817 | 1.33714 | 1.33623 | 1.33541 |
| 20 | 1.34317 | 1.34142 | 1.33992 | 1.33860 | 1.33745 | 1.33643 | 1.33551 | 1.33469 |
| 30 | 1.34208 | 1.34034 | 1.33884 | 1.33753 | 1.33638 | 1.33537 | 1.33445 | 1.33363 |
| | Wavelength (nm) | | | | | | | |
| Temp (°C) | 560 | 580 | 600 | 620 | 640 | 660 | 680 | 700 |
| 0 | 1.33494 | 1.33424 | 1.33362 | 1.33305 | 1.33251 | 1.33200 | 1.33153 | 1.33108 |
| 10 | 1.33466 | 1.33399 | 1.33336 | 1.33279 | 1.33225 | 1.33174 | 1.33127 | 1.33084 |
| 20 | 1.33397 | 1.33328 | 1.33267 | 1.33210 | 1.33156 | 1.33105 | 1.33059 | 1.33016 |
| 30 | 1.33292 | 1.33223 | 1.33162 | 1.33106 | 1.33052 | 1.33001 | 1.32955 | 1.32913 |
| | Sea Water ($S = 35‰$) Wavelength (nm) | | | | | | | |
| Temp (°C) | 400 | 420 | 440 | 460 | 480 | 500 | 520 | 540 |
| 0 | 1.35141 | 1.34961 | 1.34804 | 1.34667 | 1.34548 | 1.34442 | 1.34347 | 1.34263 |
| 10 | 1.35084 | 1.34903 | 1.34747 | 1.34612 | 1.34492 | 1.34385 | 1.34291 | 1.34207 |
| 20 | 1.34994 | 1.34814 | 1.34657 | 1.34519 | 1.34401 | 1.34295 | 1.34200 | 1.34116 |
| 30 | 1.34875 | 1.34694 | 1.34539 | 1.34404 | 1.34284 | 1.34179 | 1.34085 | 1.34000 |
| | Wavelength (nm) | | | | | | | |
| Temp (°C) | 560 | 580 | 600 | 620 | 640 | 660 | 680 | 700 |
| 0 | 1.34186 | 1.34115 | 1.34050 | 1.33992 | 1.33937 | 1.33885 | 1.33836 | 1.33791 |
| 10 | 1.34129 | 1.34061 | 1.33997 | 1.33938 | 1.33882 | 1.33830 | 1.33782 | 1.33738 |
| 20 | 1.34039 | 1.33969 | 1.33904 | 1.33845 | 1.33791 | 1.33739 | 1.33690 | 1.33644 |
| 30 | 1.33925 | 1.33855 | 1.33790 | 1.33731 | 1.33676 | 1.33624 | 1.33576 | 1.33532 |

* Data extracted from Austin and Halikas.[27]

**TABLE 5** Index of Refraction Relative to Water, $n$, of Inorganic Particles Found in Sea Water

| Substance | $n$ |
|---|---|
| Quartz | 1.16 |
| Kaolinite | 1.17 |
| Montmorillonite | 1.14 |
| Hydrated mica | 1.19 |
| Calcite | 1.11/1.24 |

retain all particulates, scattering effects within the sample cell, absorption by dissolved matter retained on the filter pad, and decomposition of pigments during the filtration process). Moreover, this methodology for determining total absorption assumes that absorption by dissolved organic matter (yellow substances) is negligible, which is not always the case. If the absorption by yellow matter, $a_y(\lambda)$, is desired, then the absorption of the *filtrate* is measured, and $a_y(\lambda)$ is taken to be $a_{\text{filtrate}}(\lambda) - a_w(\lambda)$. Several novel instruments under development[36–38] show promise for circumventing the problems inherent in the filter-pad technique as well as for making in situ measurements of total absorption which at present is difficult.[39]

## 43.11 ABSORPTION BY PURE SEA WATER

Table 2 showed the absorption for pure water over the wavelength range from 0.01 nm (x rays) to 1 m (radio waves). As is seen in the table, only the near-UV to near-IR wavelengths are of interest in hydrologic optics. Smith and Baker[32] made a careful but indirect determination of the *upper bound* of the spectral absorption coefficient of pure sea water, $a_w(\lambda)$, in the wavelength range of oceanographic interest, $200\text{ nm} \le \lambda \le 800\text{ nm}$. Their work assumed that for the clearest natural waters (1) absorption by salt or other dissolved substances was negligible, (2) the only scattering was by water molecules and salt ions, and (3) there was no inelastic scattering (i.e., no fluorescence or Raman scattering). With these assumptions the inequality (derived from radiative transfer theory)

$$a_w(\lambda) \le K_d(\lambda) - \tfrac{1}{2} b_m^{sw}(\lambda)$$

holds. Here $b_m^{sw}(\lambda)$ is the spectral scattering coefficient for pure sea water; $b_m^{sw}(\lambda)$ was taken as known (Table 10). Smith and Baker then used measured values of the diffuse attenuation function $K_d(\lambda)$ from very clear waters (e.g., Crater Lake, Oregon, U.S.A., and the Sargasso Sea) to estimate $a_w(\lambda)$. Table 6 gives their self-consistent values of $a_w(\lambda)$, $K_d(\lambda)$, and $b_m^{sw}(\lambda)$.

The Smith and Baker absorption values are widely used. However, it must be remembered that the values of $a_w(\lambda)$ in Table 6 are upper bounds; the true absorption of pure water is likely to be somewhat lower, at least at violet and blue wavelengths.[40] Smith and Baker pointed out that there are uncertainties because $K_d$, an apparent optical property, is influenced by environmental conditions. They also commented that at wavelengths below 300 nm, their values are "merely an educated guess." They estimated the accuracy of $a_w(\lambda)$ to be within +25 and −5 percent between 300 and 480 nm and +10 to −15 percent between 480 and 800 nm. Numerical simulations by Gordon[11] indicate that a more restrictive inequality,

$$a_w(\lambda) \le \frac{K_d(\lambda)}{D_0(\lambda)} - 0.62 b_m^{sw}(\lambda)$$

could be used. Here $D_0(\lambda)$ is a measurable distribution function $[D_0(\lambda) > 1]$ that corrects for the effects of sun angle and sea state on $K_d(\lambda)$ (discussed earlier). Use of the Gordon inequality could reduce the Smith and Baker absorption values by up to 20 percent at blue wavelengths. And finally, the Smith and Baker measurements were not made in optically pure water but rather in the "clearest natural waters." Even these waters contain a small amount of dissolved and particulate matter which will contribute something to both absorption and scattering.

There is evidence[41] that absorption is weakly dependent on temperature, at least in the red and near infrared ($\partial a/\partial T \sim 0.0015\text{ m}^{-1}\,^\circ\text{C}^{-1}$ at $\lambda = 600\text{ nm}$ and $\partial a/\partial T \sim 0.01\text{ m}^{-1}\,^\circ\text{C}^{-1}$ at $\lambda = 750\text{ nm}$) and perhaps also slightly dependent on salinity; these matters are under investigation.

**TABLE 6** Spectral Absorption Coefficient of Pure Sea Water, $a_w$, As Determined by Smith and Baker (Values of the molecular scattering coefficient of pure sea water, $b_m^{sw}$, and of the diffuse attenuation coefficient $K_d$ used in their computation of $a_w$ are also shown.*)

| $\lambda$ (nm) | $a_w$ ($m^{-1}$) | $b_m^{sw}$ ($m^{-1}$) | $K_d$ ($m^{-1}$) | $\lambda$ (nm) | $a_w$ ($m^{-1}$) | $b_m^{sw}$ ($m^{-1}$) | $K_d$ ($m^{-1}$) |
|---|---|---|---|---|---|---|---|
| 200 | 3.07 | 0.151 | 3.14 | 500 | 0.0257 | 0.0029 | 0.0271 |
| 210 | 1.99 | 0.119 | 2.05 | 510 | 0.0357 | 0.0026 | 0.0370 |
| 220 | 1.31 | 0.0995 | 1.36 | 520 | 0.0477 | 0.0024 | 0.0489 |
| 230 | 0.927 | 0.0820 | 0.968 | 530 | 0.0507 | 0.0022 | 0.0519 |
| 240 | 0.720 | 0.0685 | 0.754 | 540 | 0.0558 | 0.0021 | 0.0568 |
| 250 | 0.559 | 0.0575 | 0.588 | 550 | 0.0638 | 0.0019 | 0.0648 |
| 260 | 0.457 | 0.0485 | 0.481 | 560 | 0.0708 | 0.0018 | 0.0717 |
| 270 | 0.373 | 0.0415 | 0.394 | 570 | 0.0799 | 0.0017 | 0.0807 |
| 280 | 0.288 | 0.0353 | 0.306 | 580 | 0.108 | 0.0016 | 0.109 |
| 290 | 0.215 | 0.0305 | 0.230 | 590 | 0.157 | 0.0015 | 0.158 |
| 300 | 0.141 | 0.0262 | 0.154 | 600 | 0.244 | 0.0014 | 0.245 |
| 310 | 0.105 | 0.0229 | 0.116 | 610 | 0.289 | 0.0013 | 0.290 |
| 320 | 0.0844 | 0.0200 | 0.0944 | 620 | 0.309 | 0.0012 | 0.310 |
| 330 | 0.0678 | 0.0175 | 0.0765 | 630 | 0.319 | 0.0011 | 0.320 |
| 340 | 0.0561 | 0.0153 | 0.0637 | 640 | 0.329 | 0.0010 | 0.330 |
| 350 | 0.0463 | 0.0134 | 0.0530 | 650 | 0.349 | 0.0010 | 0.350 |
| 360 | 0.0379 | 0.0120 | 0.0439 | 660 | 0.400 | 0.0008 | 0.400 |
| 370 | 0.0300 | 0.0106 | 0.0353 | 670 | 0.430 | 0.0008 | 0.430 |
| 380 | 0.0220 | 0.0094 | 0.0267 | 680 | 0.450 | 0.0007 | 0.450 |
| 390 | 0.0191 | 0.0084 | 0.0233 | 690 | 0.500 | 0.0007 | 0.500 |
| 400 | 0.0171 | 0.0076 | 0.0209 | 700 | 0.650 | 0.0007 | 0.650 |
| 410 | 0.0162 | 0.0068 | 0.0196 | 710 | 0.839 | 0.0007 | 0.834 |
| 420 | 0.0153 | 0.0061 | 0.0184 | 720 | 1.169 | 0.0006 | 1.170 |
| 430 | 0.0144 | 0.0055 | 0.0172 | 730 | 1.799 | 0.0006 | 1.800 |
| 440 | 0.0145 | 0.0049 | 0.0170 | 740 | 2.38 | 0.0006 | 2.380 |
| 450 | 0.0145 | 0.0045 | 0.0168 | 750 | 2.47 | 0.0005 | 2.47 |
| 460 | 0.0156 | 0.0041 | 0.0176 | 760 | 2.55 | 0.0005 | 2.55 |
| 470 | 0.0156 | 0.0037 | 0.0175 | 770 | 2.51 | 0.0005 | 2.51 |
| 480 | 0.0176 | 0.0034 | 0.0194 | 780 | 2.36 | 0.0004 | 2.36 |
| 490 | 0.0196 | 0.0031 | 0.0212 | 790 | 2.16 | 0.0004 | 2.16 |
| | | | | 800 | 2.07 | 0.0004 | 2.07 |

* Reproduced from Smith and Baker,[32] with permission.

## 43.12 ABSORPTION BY DISSOLVED ORGANIC MATTER

Absorption by yellow matter is reasonably well described by the model[42]

$$a_y(\lambda) = a_y(\lambda_0) \exp\left[-0.014(\lambda - \lambda_0)\right]$$

over the range $350\,\text{nm} \le \lambda \le 700\,\text{nm}$. Here $\lambda_0$ is a reference wavelength usually chosen to be $\lambda_0 = 440\,\text{nm}$ and $a_y(\lambda_0)$ is the absorption due to yellow matter at the reference wavelength. The value of $a_y(\lambda)$ of course depends on the concentration of yellow matter in the water. The exponential decay constant depends on the relative proportion of specific types of yellow matter; other studies have found exponents of $-0.014$ to $-0.019$ (Roesler et al.,[43] table 1). Both total concentration and proportions are highly variable. Table 7 gives measured values of $a_y(440)$ for selected waters. Because of the variability in yellow

**TABLE 7** Measured Absorption Coefficient at $\lambda = 440\,\text{nm}$ Due to Yellow Matter, $a_y(440\,\text{nm})$, for Selected Waters*

| Water body | $a_y(440\,\text{nm})$ ($\text{m}^{-1}$) |
|---|---|
| Oceanic waters | |
| Sargasso Sea | ≈0 |
| off Bermuda | 0.01 |
| Gulf of Guinea | 0.024–0.113 |
| oligotrophic Indian Ocean | 0.02 |
| mesotrophic Indian Ocean | 0.03 |
| eutrophic Indian Ocean | 0.09 |
| Coastal and estuarine waters | |
| North Sea | 0.07 |
| Baltic Sea | 0.24 |
| Rhone River mouth, France | 0.086–0.572 |
| Clyde River estuary, Australia | 0.64 |
| Lakes and rivers | |
| Crystal Lake, Wisconsin, U.S.A. | 0.16 |
| Lake George, Australia | 0.69–3.04 |
| Lake George, Uganda | 3.7 |
| Carrao River, Venezuela | 12.44 |
| Lough Napeast, Ireland | 19.1 |

* Condensed from Kirk,[8] with permission.

matter concentrations, the values found in Table 7 have little general validity even for the particular water bodies sampled, but they do serve to show representative values and the range of influence of yellow matter in determining the total absorption. Although the above model allows the determination of spectral absorption by yellow matter if the absorption is known at one wavelength, no model yet exists that allows for the direct determination of $a_y(\lambda)$ from given concentrations of yellow matter constituents.

## 43.13 ABSORPTION BY PHYTOPLANKTON

Phytoplankton cells are strong absorbers of visible light and therefore play a major role in determining the absorption properties of natural waters. Absorption by phytoplankton occurs in various photosynthetic pigments of which the chlorophylls are best known to nonspecialists. Absorption by chlorophyll itself is characterized by strong absorption bands in the blue and in the red (peaking at $\lambda \approx 430$ and 665 nm, respectively, for chlorophyll *a*), with very little absorption in the green. Chlorophyll occurs in all plants, and its concentration in milligrams of chlorophyll per cubic meter of water is commonly used as the relevant optical measure of phytoplankton abundance. (The term "chlorophyll concentration" usually refers to the sum of chlorophyll *a*, the main pigment in phytoplankton cells, and the related pigment pheophytin *a*.) Chlorophyll concentrations for various waters range from 0.01 mg $\text{m}^{-3}$ in the clearest open ocean waters to 10 mg $\text{m}^{-3}$ in productive coastal upwelling regions to 100 mg $\text{m}^{-3}$ in eutrophic estuaries or lakes. The globally averaged, near-surface, open-ocean value is in the neighborhood of 0.5 mg $\text{m}^{-3}$.

The absorbing pigments are not evenly distributed within phytoplankton cells but are

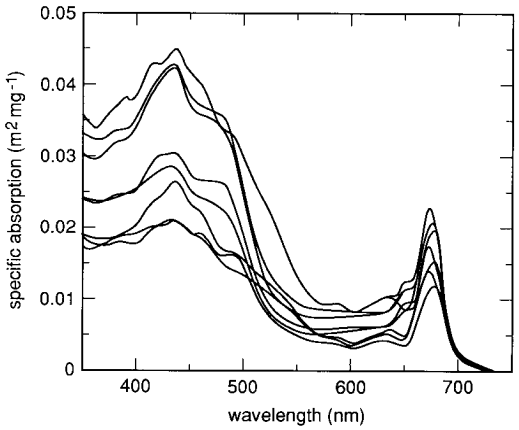


**FIGURE 6** Chlorophyll-specific spectral absorption coefficients for eight species of phytoplankton. (*Redrawn from Sathyendranath et al.,*[44] *with permission.*)

localized into small "packages" (chloroplasts) which are distributed nonrandomly throughout the cell. This localized distribution of pigments means[8] that the spectral absorption by a phytoplankton cell or by a collection of cells in water is "flatter" (has less-pronounced peaks and reduced overall absorption) than if the pigments were uniformly distributed throughout the cell or throughout the water. This so-called "pigment packaging effect" is a major source of both inter- and intraspecies variability in spectral absorption by phytoplankton. This is because the details of the pigment packaging within cells depend not only on species but also on a cell's size and physiological state (which in turn depends on environmental factors such as ambient lighting and nutrient availability). Another source of variability in addition to chlorophyll *a* concentration and packaging is changes in pigment composition (the relative proportions of accessory pigments, namely chlorophylls *b* and *c,* pheopigments, biliproteins, and carotenoids) since each pigment displays a characteristic absorption curve.

A qualitative feel for the nature of phytoplankton absorption can be obtained from Fig. 6 which is based on absorption measurements from eight different single-species laboratory phytoplankton cultures.[44] Measured spectral absorption coefficients for the eight cultures, $a_i(\lambda)$, $i = 1$ to 8, were first reduced by subtracting $a_i(737)$ to remove the effects of absorption by detritus and cell constituents other than pigments: the assumption is that pigments do not absorb at $\lambda = 737$ nm and that the residual absorption is wavelength independent (which is a crude approximation). The resulting curves were then normalized by the chlorophyll concentrations of the respective cultures to generate the *chlorophyll-specific spectral absorption* curves for phytoplankton, $a_i^*(\lambda)$:

$$a_i^*(\lambda) = \frac{a_i(\lambda) - a_i(737)}{C_i} \qquad \frac{\mathrm{m}^{-1}}{\mathrm{mg\,m}^{-3}} = \mathrm{m}^2\,\mathrm{mg}^{-1}$$

which are plotted in Fig. 6.

Several general features of phytoplankton absorption are seen in Fig. 6:

1. There are distinct absorption peaks at $\lambda \approx 440$ and 675 nm.
2. The blue peak is one to three times as high as the red one (for a given species) due to the contribution of accessory pigments to absorption in the blue.
3. There is relatively little absorption between 550 and 650 nm, with the absorption minimum near 600 nm being 10 to 30 percent of the value at 440 nm.

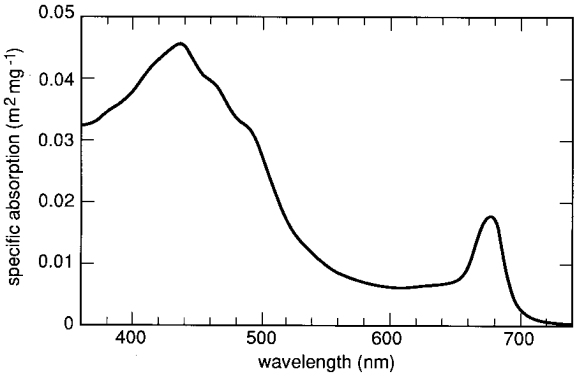


**FIGURE 7** Average chlorophyll-specific spectral absorption coefficient for 14 species of phytoplankton. (*Redrawn from Morel,*[45] *with permission.*)

Similar analysis by Morel[45] yielded the average specific absorption curve shown in Fig. 7. Morel's curve is an average of spectra from 14 cultured phytoplankton species. The Morel curve is qualitatively the same as the curves of Fig. 6 and is as good a candidate as any for being called a ''typical'' phytoplankton specific absorption curve. The $a^*(\lambda)$ values of Fig. 7 are tabulated in Table 8 for reference.

## 43.14 ABSORPTION BY ORGANIC DETRITUS

Only recently has it become possible to determine the relative contributions of living phytoplankton and nonliving detritus to the total absorption by particulates. Iturriaga and Siegel[46] used microspectrophotometric techniques capable of measuring the spectral absorption of individual particles as small as 3 μm diameter to examine the absorption properties of particulates from Sargasso sea waters. Roesler et al.[43] employed a standard filter-pad technique with measurements made before and after pigments were chemically extracted to distinguish between absorption by pigmented and nonpigmented particles from fjord waters in the San Juan Islands, Washington, U.S.A. Each of these dissimilar techniques applied to particles from greatly different waters found very similar absorption spectra for nonpigmented organic particles derived from phytoplankton.

Figure 8 shows the microspectrophotometrically determined contributions of absorption by phytoplankton, $a_{ph}(\lambda)$, and of absorption by detritus, $a_{det}(\lambda)$, to the independently measured (by the filter-pad technique) total particulate absorption, $a_p(\lambda)$, for two depths at the same Atlantic location. The small residual, $\Delta a_p(\lambda) = a_p(\lambda) - a_{ph}(\lambda) - a_{det}(\lambda)$ shown in the figure is attributed either to errors in the determination of the phytoplankton and detrital parts (particles smaller than ~3 μm were not analyzed) or to contamination by dissolved organic matter of the filter-pad measurements of total particulate absorption. Note that at the shallow depth the phytoplankton are relatively more important at blue wavelengths whereas the detritus is slightly more important at the deeper depth. There is no generality in this result (other locations showed the reverse)—it merely illustrates the variability possible in water samples taken only 60 vertical meters apart.

The important feature to note in Fig. 8 is the general shape of the spectral absorption curve for detritus. Roesler et al. found essentially identical curves in their determination of $a_{det}(\lambda)$. These curves are reminiscent of the absorption curves for yellow matter and, indeed, Roesler et al. found that the model

$$a_{det}(\lambda) = a_{det}(400) \exp\left[-0.011(\lambda - 400)\right]$$

**TABLE 8** Average Chlorophyll-Specific Spectral Absorption Coefficient $a^*$ for 14 Species of Phytoplankton As Plotted in Fig. 7 (The standard deviation is ~30% of the mean except in the vicinity of 400 nm, where it is ~50%.*)

| $\lambda$ (nm) | $a^*$ ($m^2\,mg^{-1}$) | $\lambda$ (nm) | $a^*$ ($m^2\,mg^{-1}$) | $\lambda$ (nm) | $a^*$ ($m^2\,mg^{-1}$) |
|---|---|---|---|---|---|
| 400 | 0.0394 | 500 | 0.0274 | 600 | 0.0053 |
| 405 | 0.0395 | 505 | 0.0246 | 605 | 0.0053 |
| 410 | 0.0403 | 510 | 0.0216 | 610 | 0.0054 |
| 415 | 0.0417 | 515 | 0.0190 | 615 | 0.0057 |
| 420 | 0.0429 | 520 | 0.0168 | 620 | 0.0059 |
| 425 | 0.0439 | 525 | 0.0151 | 625 | 0.0061 |
| 430 | 0.0448 | 530 | 0.0137 | 630 | 0.0063 |
| 435 | 0.0452 | 535 | 0.0125 | 635 | 0.0064 |
| 440 | 0.0448 | 540 | 0.0115 | 640 | 0.0064 |
| 445 | 0.0436 | 545 | 0.0106 | 645 | 0.0066 |
| 450 | 0.0419 | 550 | 0.0098 | 650 | 0.0071 |
| 455 | 0.0405 | 555 | 0.0090 | 655 | 0.0084 |
| 460 | 0.0392 | 560 | 0.0084 | 660 | 0.0106 |
| 465 | 0.0379 | 565 | 0.0078 | 665 | 0.0136 |
| 470 | 0.0363 | 570 | 0.0073 | 670 | 0.0161 |
| 475 | 0.0347 | 575 | 0.0068 | 675 | 0.0170 |
| 480 | 0.0333 | 580 | 0.0064 | 680 | 0.0154 |
| 485 | 0.0322 | 585 | 0.0061 | 685 | 0.0118 |
| 490 | 0.0312 | 590 | 0.0058 | 690 | 0.0077 |
| 495 | 0.0297 | 595 | 0.0055 | 695 | 0.0046 |
| | | | | 700 | 0.0027 |

* Data courtesy of A. Morel[45].

provides a satisfactory fit to detrital absorption curves. Other studies have found coefficients of $-0.006$ to $-0.014$ (Roesler et al.,[43] table 1) instead of $-0.011$.

## 43.15 BIO-OPTICAL MODELS FOR ABSORPTION

Depending on the concentrations of dissolved substances, phytoplankton, and detritus, the total spectral absorption coefficient of a given water sample can range from almost identical to that of pure water to one which shows orders-of-magnitude greater absorption than pure water, especially at blue wavelengths. Figure 9 shows some $a(\lambda)$ profiles from various natural waters. Figure 9*a* shows absorption profiles measured in phytoplankton-dominated waters where chlorophyll concentrations ranged from $C = 0.2$ to $18.4\,mg\,m^{-3}$. In essence, the absorption is high in the blue because of absorption by phytoplankton pigments and high in the red because of absorption by the water. Figure 9*b* shows the absorption at three locations where $C \approx 2\,mg\,m^{-3}$ but where the scattering coefficient $b$ varied from 1.55 to $3.6\,m^{-1}$ indicating that nonpigmented particles were playing an important role in determining the shape of $a(\lambda)$. Figure 9*c* shows curves from waters rich in yellow matter, which is causing the high absorption in the blue. One of the goals of bio-optics is to develop predictive models for absorption curves such as those seen in Fig. 9.

*Case 1 waters* are waters in which the concentration of phytoplankton is high compared to nonbiogenic particles.[47] Absorption by chlorophyll and related pigments therefore plays

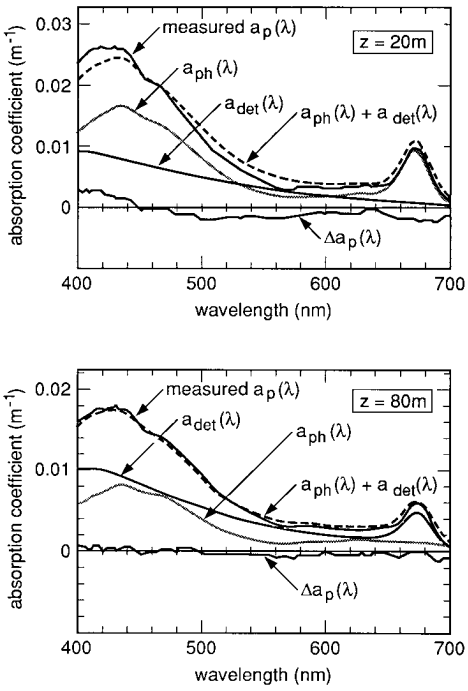


**FIGURE 8** Examples of the relative contributions of absorption by phytoplankton $a_{ph}(\lambda)$, and by organic detritus $a_{det}(\lambda)$, to the total particulate absorption $a_p(\lambda)$, from Sargasso Sea waters. (*Redrawn from Iturriaga and Siegel,*[46] *with permission.*)

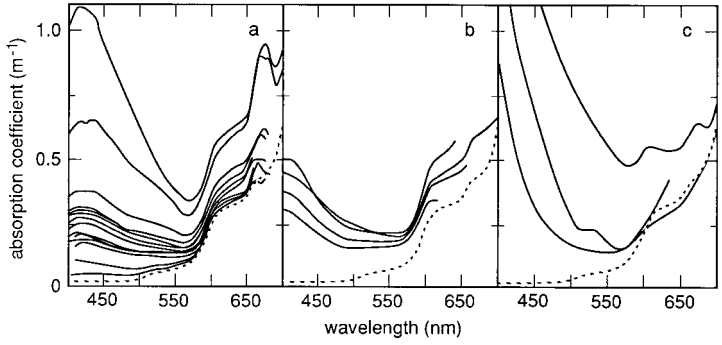


**FIGURE 9** Examples of spectral absorption coefficients $a(\lambda)$ for various waters. Panel (*a*) shows $a(\lambda)$ for waters dominated by phytoplankton, panel (*b*) is for waters with a high concentration of nonpigmented particles, and panel (*c*) is for waters rich in yellow matter. (*Based on Prieur and Sathyendranath,*[48] *with permission.*)

a major role in determining the total absorption coefficient in such waters, although detritus and dissolved organic matter derived from the phytoplankton also contribute to absorption in case 1 waters. Case 1 water can range from very clear (oligotrophic) water to very turbid (eutrophic) water, depending on the phytoplankton concentration. *Case 2 waters* are "everything else," namely, waters where inorganic particles or dissolved organic matter from land drainage dominate so that absorption by pigments is relatively less important in determining the total absorption. (The case 1 and 2 classifications must not be confused with the Jerlov water *types* 1 and 2, discussed later.) Roughly 98 percent of the world's open ocean and coastal waters fall into the case 1 category, and therefore almost all bio-optical research has been directed toward these phytoplankton-dominated waters. However, near-shore and estuarine case 2 waters are disproportionately important to human interests such as recreation, fisheries, and military operations.

Prieur and Sathyendranath[48] developed a pioneering bio-optical model for the spectral absorption coefficient of case 1 waters. Their model was statistically derived from 90 sets of spectral absorption data taken in various case 1 waters and included absorption by phytoplankton pigments, by nonpigmented organic particles derived from deceased phytoplankton, and by yellow matter derived from decayed phytoplankton. The contribution of phytoplankton to the total absorption was parametrized in terms of the chlorophyll concentration $C$ (i.e., chlorophyll $a$ plus pheophytin $a$). The contributions of nonpigmented particles and of yellow matter were parametrized in terms of both the chlorophyll concentration and the total scattering coefficient at $\lambda = 550$ nm, $b(550)$. The essence of the Prieur-Sathyendranath model is contained in a more recent and simpler variant given by Morel[6]:

$$a(\lambda) = [a_w(\lambda) + 0.06a_c^{*\prime}(\lambda)C^{0.65}][1 + 0.2 \exp(-0.014(\lambda - 440))] \quad (1)$$

Here $a_w(\lambda)$ is the absorption coefficient of pure water and $a_c^{*\prime}(\lambda)$ is a nondimensional, statistically derived chlorophyll-specific absorption coefficient; $a_w(\lambda)$ and $a_c^{*\prime}(\lambda)$ values are given in Table 9 [these $a_w(\lambda)$ values are slightly different than those of Table 6]. When $C$ is expressed in mg m$^{-3}$ and $\lambda$ is in nm, the resulting $a(\lambda)$ is in m$^{-1}$.

Another simple bio-optical model for absorption has been developed independently by Kopelevich.[49] It has the form[50]

$$a(\lambda) = a_w(\lambda) + C[a_c^0(\lambda) + 0.1 \exp[-0.015(\lambda - 400)]$$

**TABLE 9** Absorption by Pure Sea Water, $a_w$, and the Nondimensional Chlorophyll-Specific Absorption Coefficient $a_c^{*\prime}$ Used in The Prieur-Sathyendranath-Morel Model for the Spectral Absorption Coefficient $a(\lambda)$*

| $\lambda$ (nm) | $a_w$ (m$^{-1}$) | $a_c^{*\prime}$ | $\lambda$ (nm) | $a_w$ (m$^{-1}$) | $a_c^{*\prime}$ | $\lambda$ (nm) | $a_w$ (m$^{-1}$) | $a_c^{*\prime}$ |
|---|---|---|---|---|---|---|---|---|
| 400 | 0.018 | 0.687 | 500 | 0.026 | 0.668 | 600 | 0.245 | 0.236 |
| 410 | 0.017 | 0.828 | 510 | 0.036 | 0.618 | 610 | 0.290 | 0.252 |
| 420 | 0.016 | 0.913 | 520 | 0.048 | 0.528 | 620 | 0.310 | 0.276 |
| 430 | 0.015 | 0.973 | 530 | 0.051 | 0.474 | 630 | 0.320 | 0.317 |
| 440 | 0.015 | 1.000 | 540 | 0.056 | 0.416 | 640 | 0.330 | 0.334 |
| 450 | 0.015 | 0.944 | 550 | 0.064 | 0.357 | 650 | 0.350 | 0.356 |
| 460 | 0.016 | 0.917 | 560 | 0.071 | 0.294 | 660 | 0.410 | 0.441 |
| 470 | 0.016 | 0.870 | 570 | 0.080 | 0.276 | 670 | 0.430 | 0.595 |
| 480 | 0.018 | 0.798 | 580 | 0.108 | 0.291 | 680 | 0.450 | 0.502 |
| 490 | 0.020 | 0.750 | 590 | 0.157 | 0.282 | 690 | 0.500 | 0.329 |
| | | | | | | 700 | 0.650 | 0.215 |

* Condensed with permission from Prieur and Sathyendranath,[48] who give values every 5 mm.

where $a_c^0(\lambda)$ is the chlorophyll-specific absorption coefficient for phytoplankton ($m^2\,mg^{-1}$), and $a_w(\lambda)$ and $C$ are defined as for Eq. (1). The Kopelevich model as presently used[49] takes $a_w(\lambda)$ from Smith and Baker[32] (Table 6) and takes $a_c^0(\lambda)$ from Yentsch.[51]

Although these and similar bio-optical models for absorption are frequently used, caution is advised in their application. Both models assume that the absorption by yellow matter covaries with that due to phytoplankton; i.e., each implies that a fixed percentage of the total absorption at a given wavelength always comes from yellow matter. The general validity of this assumption is doubtful even for open ocean waters: Bricaud et al.[42] show data (fig. 5) for which $a(375)$, used as an index for yellow matter concentration, is uncorrelated with chlorophyll concentration even in oceanic regions uninfluenced by freshwater runoff. Gordon[52] has developed a model that avoids assuming any relation between yellow matter and phytoplankton. However, his model becomes singular as $C \to 0.01\,mg\,m^{-3}$ and cannot be expected to work well for $C$ much less than $0.1\,mg\,m^{-3}$. The Kopelevich model has the chlorophyll contribution proportional to $C$, whereas the Morel model has $C^{0.65}$. The exponent of 0.65 is probably closer to reality, since it reflects a change in the relative contributions to absorption by phytoplankton and by detritus as the chlorophyll concentration changes (absorption by detritus is relatively more important at low chlorophyll concentrations[52]). Moreover, the chlorophyll-specific absorption curve of Yentsch[51] used in the Kopelevich model is based on laboratory cultures of phytoplankton, whereas the later work by Prieur and Sathyendranath used in situ observations to derive the $a_c^{*\prime}(\lambda)$ values of Table 9—an additional point in favor of Eq. (1). Either of these bio-optical models is useful but clearly imperfect. They may (or may not) give correct *average* values, but they give no information about the *variability* of $a(\lambda)$. It can be anticipated that the simple models now available will be replaced, perhaps by models designed for specific regions and seasons, as better understanding of the variability inherent in spectral absorption is achieved.

## 43.16 MEASUREMENT OF SCATTERING

Scattering in natural waters is caused both by small scale ($\ll\lambda$) density fluctuations attributable to random molecular motions and by the ubiquitous large ($>\lambda$) organic and inorganic particles. Scattering by water molecules (and salt ions, in seawater) determines the minimum values for the scattering properties. However, as is the case for absorption, the scattering properties of natural waters are greatly modified by the particulate matter that is always present.

Scattering measurements are even more difficult than absorption measurements. The conceptual design of an instrument for measuring the volume scattering function $\beta(\psi, \lambda)$ is no more complicated than Fig. 2 and the defining equation $\beta(\psi, \lambda) = I_s(\psi, \lambda)/[E_i(\lambda)\,\Delta V]$: a collimated beam of known irradiance $E_i$ illuminates a given volume of water $\Delta V$ and the scattered intensity $I_s$ is measured as a function of scattering angle and wavelength. However, the engineering of instruments capable of the in situ determination of $\beta(\psi, \lambda)$ is quite difficult. The magnitude of the scattered intensity typically increases by five or six orders of magnitude in going from $\psi = 90°$ to $\psi = 0.1°$ for a given natural water sample, and scattering at a given angle $\psi$ can vary by two orders of magnitude among water samples. The required dynamic range of an instrument is therefore great. Corrections must be made for absorption within the sample volume and also along the incident and scattered beam paths for in situ instruments. The rapid change in $\beta(\psi, \lambda)$ at small scattering angles requires very precise alignment of the optical elements, but rolling ships seem designed to knock things out of alignment. Because of these design difficulties only a few one-of-a-kind instruments have been built for in situ measurement of the volume scattering function, and measurements of $\beta(\psi, \lambda)$ are not routinely made. Petzold[53] gives the details of two such

instruments, one for small scattering angles ($\psi = 0.085$, 0.17, and 0.34°) and one for larger angles ($10° \leq \psi \leq 170°$); these are the instruments used to obtain the data presented in Sec. 43.18. Other instruments are referenced in Kirk[8] and in Jerlov.[29]

Commercial instruments are available for laboratory measurement of $\beta(\psi, \lambda)$ at fixed scattering angles (e.g., $\psi$ every 5° from ~20 to ~160°). These instruments are subject to their own problems, such as degradation of samples between the times of collection and measurement. Moreover, measurements of $\beta(\psi, \lambda)$ over a limited range of $\psi$ are not sufficient for determination of $b(\lambda)$ by integration. In practice, the scattering coefficient $b(\lambda)$ is usually determined by the conservation of energy relation $b(\lambda) = c(\lambda) - a(\lambda)$ after measurements of beam attenuation and absorption have been made.

Both in situ and laboratory instruments sample (~$cm^3$) volumes of water and therefore may fail to detect the presence of optically significant large aggregates (marine snow) if such particles are too few in number to be reliably captured in the sample volume. However, such particles can affect the scattering properties of large volumes of water (e.g., as seen in remote sensing or underwater visibility studies).

Measurements at near forward ($\psi < 1°$) and near backward ($\psi > 179°$) angles are exceptionally difficult to make, yet the behavior of $\beta(\psi, \lambda)$ at these extreme angles is of considerable interest. Accurate determination of $\beta$ at small angles is crucial to the determination of $b$ by integration since typically one-half of all scattering takes place at angles of less than a few degrees. Scattering at small angles is important in underwater imaging and it is of theoretical interest for its connections to scattering theory, particle optical properties, and particle size distributions. The behavior of $\beta$ very near $\psi = 180°$ is important in laser remote-sensing applications.

Spinrad et al.[54] and Padmabandu and Fry[55] have reported measurements at very small angles on suspensions of polystyrene spheres but no such measurements have been published for natural water samples. The Padmabandu and Fry technique is notable in that it allows the measurement of $\beta$ at $\psi = 0°$ exactly by use of the coupling of two coherent beams in a photorefractive crystal to measure the phase shift that corresponds to 0° scattering. Measurement of $\beta(0, \lambda)$ is of theoretical interest because of its relation to attenuation via the optical theorem. Enhanced backscatter has been reported[56] in suspensions of latex spheres; a factor-of-two increase in scattered intensity between $\psi = 179.5$ and 180.0° is typical. Whether or not such backscattering enhancement ever occurs in natural waters is a subject of heated debate.

## 43.17 SCATTERING BY PURE WATER AND BY PURE SEA WATER

Morel[57] has reviewed in detail the theory and observations pertaining to scattering by pure water and by pure sea water. In pure water random molecular motions give rise to rapid fluctuations in the number of molecules in a given volume $\Delta V$, where $\Delta V$ is small compared to the wavelength of light but large compared to atomic scales (so that the liquid within the volume is adequately described by statistical thermodynamics). The Einstein-Smoluchowski theory of scattering relates these fluctuations in molecular number density to associated fluctuations in the index of refraction, which give rise to scattering. In sea water the basic theory is the same but random fluctuations in the concentrations of the various ions ($Cl^-$, $Na^+$, etc.) give somewhat greater index of refraction fluctuations, and hence greater scattering. The net result of these considerations is that the volume scattering function for either pure water or for pure sea water has the form

$$\beta_w(\psi, \lambda) = \beta_w(90°, \lambda_0)\left(\frac{\lambda_0}{\lambda}\right)^{4.32}(1 + 0.835\cos^2\psi) \qquad m^{-1}\,sr^{-1} \tag{2}$$

which is reminiscent of the form for Rayleigh scattering. The wavelength dependence of

**TABLE 10** The Volume Scattering Function at $\psi = 90°$, $\beta_w(90°, \lambda)$, and the Scattering Coefficient $b_w(\lambda)$ for Pure Water and for Pure Sea Water ($S = 35$–39‰)*

| | Pure water | | Pure sea water | |
|---|---|---|---|---|
| $\lambda$ (nm) | $\beta_w(90°)$ ($10^{-4}$ m$^{-1}$ sr$^{-1}$) | $b_w$† ($10^{-4}$ m$^{-1}$) | $\beta(90°)$ ($10^{-4}$ m$^{-1}$ sr$^{-1}$) | $b_w$† ($10^{-4}$ m$^{-1}$) |
| 350 | 6.47 | 103.5 | 8.41 | 134.5 |
| 375 | 4.80 | 76.8 | 6.24 | 99.8 |
| 400 | 3.63 | 58.1 | 4.72 | 75.5 |
| 425 | 2.80 | 44.7 | 3.63 | 58.1 |
| 450 | 2.18 | 34.9 | 2.84 | 45.4 |
| 475 | 1.73 | 27.6 | 2.25 | 35.9 |
| 500 | 1.38 | 22.2 | 1.80 | 28.8 |
| 525 | 1.12 | 17.9 | 1.46 | 23.3 |
| 550 | 0.93 | 14.9 | 1.21 | 19.3 |
| 575 | 0.78 | 12.5 | 1.01 | 16.2 |
| 600 | 0.68 | 10.9 | 0.88 | 14.1 |

* Reproduced from Morel,[57] with permission.
† Computed from $b(\lambda) = 16.0\beta(90°, \lambda)$.

$\lambda^{-4.32}$ rather than $\lambda^{-4}$ (for Rayleigh scattering) results from the wavelength dependence of the index of refraction. The 0.835 factor is attributable to the anisotropy of the water molecules. The corresponding phase function is

$$\tilde{\beta}_w(\psi) = 0.06225(1 + 0.835\cos^2\psi) \qquad \text{sr}^{-1}$$

and the total scattering coefficient $b_w(\lambda)$ is given by

$$b_w(\lambda) = 16.06\left(\frac{\lambda_0}{\lambda}\right)^{4.32}\beta_w(90°, \lambda_0) \qquad \text{m}^{-1} \tag{3}$$

Table 10 gives values of $\beta_w(90°, \lambda)$ and $b_w(\lambda)$ for selected wavelengths for both pure water and pure sea water ($S = 35$–39‰). Note that the pure sea water values are about 30 percent greater than the pure water values at all wavelengths. Table 11 shows the dependence of $b_w(546)$ on pressure, temperature, and salinity. Note that molecular

**TABLE 11** Computed Scattering Coefficient $b$ of Pure Water ($S = 0$) and of Pure Sea Water ($S = 35$‰) at $\lambda = 546$ nm As a Function of Temperature $T$ and Pressure $p$ (Numbers in the body of the table have units of m$^{-1}$.*)

| | $p = 10^5$ Pa (1 atm) | | $p = 10^7$ Pa (100 atm) | | $p = 10^8$ Pa (1000 atm) | |
|---|---|---|---|---|---|---|
| $T$ (°C) | $S = 0$ | $S = 35$‰ | $S = 0$ | $S = 35$‰ | $S = 0$ | $S = 35$‰ |
| 0 | 0.00145 | 0.00195 | 0.00140 | 0.00192 | 0.00110 | 0.00167 |
| 10 | 0.00148 | 0.00203 | 0.00143 | 0.00200 | 0.00119 | 0.00176 |
| 20 | 0.00149 | 0.00207 | 0.00147 | 0.00204 | 0.00125 | 0.00183 |
| 40 | 0.00150 | 0.00213 | 0.00149 | 0.00212 | 0.00136 | 0.00197 |

* Data extracted from the more extensive table of Shifrin,[58] with permission.

scattering decreases as decreasing temperature or increasing pressure reduce the small-scale fluctuations.

## 43.18 SCATTERING BY PARTICLES

Heroic efforts are required to obtain water of sufficient purity that a Rayleigh-like volume scattering function is observed. As soon as there is a slight amount of particulate matter in the water—always the case for even the clearest natural water—the volume scattering function becomes highly peaked in the forward direction, and the scattering coefficient increases by at least a factor of ten.

Even for the most numerous oceanic particles (e.g., colloids at a concentration of $10^{15}\ m^{-3}$) the average distance between particles is greater than ten wavelengths of visible light. For the optically most significant phytoplankton the average separation is thousands of wavelengths. Moreover, these particles usually are randomly distributed and oriented. Ocean water therefore can be treated as a very dilute suspension of random scatterers and consequently the intensity of light scattered by an ensemble of particles is given by the sum of the intensities due to the individual particles. Coherent scattering effects are negligible except perhaps at extremely small scattering angles.[58] An overview of scattering by particles is given in Chap. 6 by Bohren in this *Handbook.*

The conrtibution of the particulate matter to the total volume scattering function $\beta(\psi, \lambda)$ is obtained from

$$\beta_p(\psi, \lambda) \equiv \beta(\psi, \lambda) - \beta_w(\psi, \lambda)$$

Here the subscript p refers to particles, and w refers to pure water (if $\beta$ is measured in fresh water) or pure sea water (for oceanic measurements). Figure 10 shows several particle volume scattering functions determined from in situ measurements of $\beta(\psi, \lambda)$ in a variety of waters ranging from very clear to very turbid. The particles cause at least a four-order-of-magnitude increase in scattering between $\psi \approx 90°$ and $\psi \approx 1°$. The contribution of molecular scattering to the total is therefore completely negligible except at backscattered directions ($\psi \geq 90°$) in the clearest natural waters. The top curve in Fig. 10 is shown for small scattering angles in Fig. 11. The scattering function shows no indication of "flattening out" even at angles as small as 0.5°. Note that the scattering function increases by a factor of 100 over only a one-degree range of scattering angle.

Highly peaked forward scattering such as that seen in Figs. 10 and 11 is characteristic of diffraction-dominated scattering in a polydisperse system. Scattering by refraction and reflection from particle surfaces becomes important at large scattering angles ($\psi \gtrsim 15°$). Mie scattering calculations are well able to reproduce observed volume scattering functions given the proper optical properties and size distributions. Early efforts along these lines are seen in Kullenberg[59] and in Brown and Gordon.[60] Brown and Gordon were unable to reproduce observed backscattering values using measured particle size distributions. However, their instruments were unable to detect submicrometer particles. They found that the Mie theory properly predicted backscattering if they assumed the presence of numerous, submicrometer, low-index-of-refraction particles. It is reasonable to speculate that bacteria and the recently discovered colloidal particles are the particles whose existence was inferred by Brown and Gordon. Recent Mie scattering calculations[61] have used three-layered spheres to model the structure of phytoplankton (cell wall, chloroplasts, and cytoplasm core) and have used polydisperse mixtures of both organic and inorganic particles.

The most carefully made and widely cited scattering measurements are found in Petzold.[53] Figure 12 shows three of his $\beta(\psi, \lambda)$ curves displayed on a log-log plot to emphasize the forward scattering angles. The instruments had a spectral response

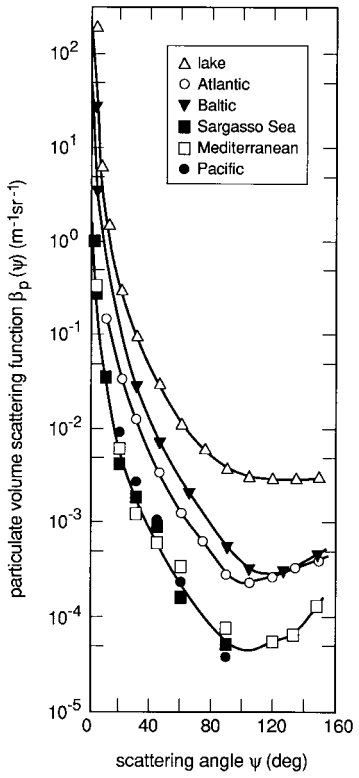


**FIGURE 10** Particulate volume scattering functions $\beta_p(\psi, \lambda)$ determined from *in situ* measurements in various waters; wavelengths vary. (*Redrawn from Kullenberg,*[59] *with permission.*)

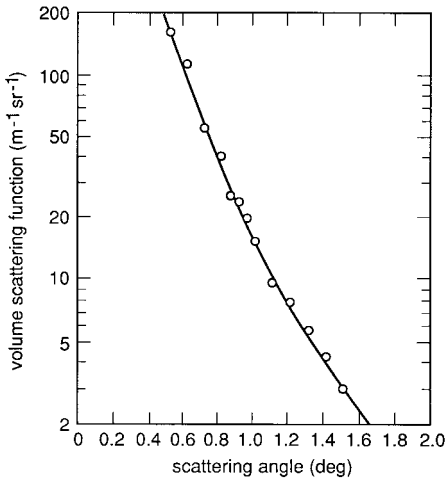


**FIGURE 11** Detail of the forward scattering values of the "lake" volume scattering function seen in the top curve of Fig. 10. (*Redrawn from Preisendorfer.*[2])

centered at $\lambda = 514$ nm with an FWHM of 75 nm. The top curve was obtained in the very turbid water of San Diego Harbor, California; the center curve comes from near-shore coastal water in San Pedro Channel, California; and the bottom curve is from very clear water in the Tongue of the Ocean, Bahama Islands. The striking feature of these volume scattering functions (and those of Fig. 10) from very different waters is the similarity of their shapes. Although the scattering coefficients $b$ of the curves in Fig. 12 vary by a factor of 50 (Table 13), the uniform shapes suggest that it is reasonable to define a "typical" particle phase function $\tilde{\beta}_p(\psi, \lambda)$. This has been done[62] with three sets of Petzold's data from waters with a high particulate load (one set being the top curve of Fig. 12), as follows: (1) subtract $\beta_w(\psi, \lambda)$ from each curve to get three particle volume scattering functions $\beta_p^i(\psi, \lambda)$, $i = 1, 2, 3$; (2) compute three particle phase functions via $\tilde{\beta}_p^i(\psi, \lambda) = \beta_p^i(\psi, \lambda)/b^i(\lambda)$; (3) average the three particle phase functions to define the typical particle phase function $\tilde{\beta}_p(\psi, \lambda)$. Table 12 displays the three Petzold volume scattering functions plotted in Fig. 12, the volume scattering function for pure sea water, and the average particle phase function computed as just described. This particle phase function satisfies the normalization $2\pi \int_0^\pi \tilde{\beta}_p(\psi, \lambda) \sin \psi \, d\psi = 1$ if a behavior of $\tilde{\beta}_p \sim \psi^{-m}$ is assumed for $\psi < 0.1°$ ($m$ is a positive constant between zero and two, determined from $\tilde{\beta}_p$ at the smallest measured angles), and a trapezoidal rule integration is used for $\psi \geq 0.1°$, with linear interpolation used between the tabulated values. This average particle phase

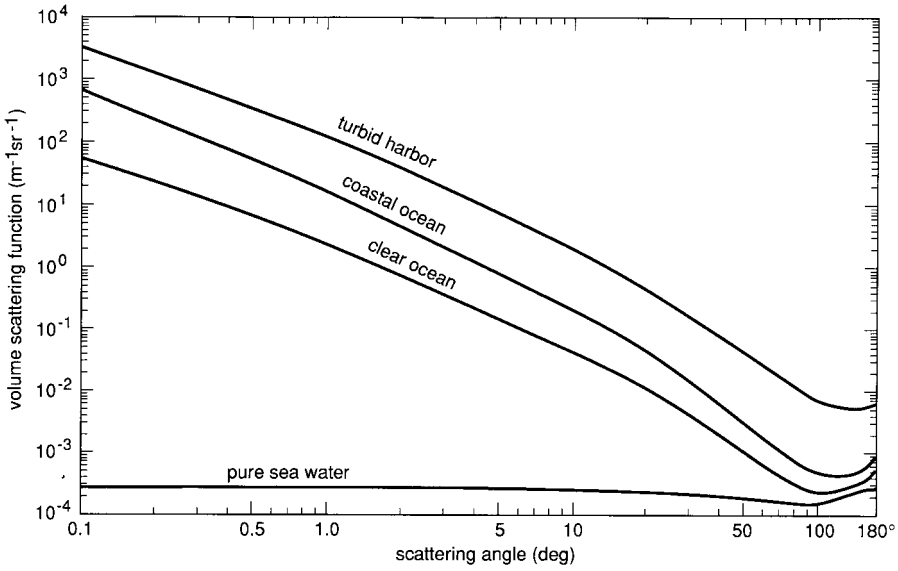


**FIGURE 12** Measured volume scattering functions from three different natural waters and the computed volume scattering function for pure sea water, all at $\lambda = 514$ nm. (*Redrawn from Petzold.*[53])

function is adequate for many radiative transfer calculations. However, the user must remember that significant deviations from the average can be expected in nature (e.g., in waters with abnormally high numbers of either large or small particles), although the details of such deviations have not been quantified.

Table 13 compares several inherent optical properties for pure sea water and for the three Petzold water samples of Fig. 12 and Table 12. These data show how greatly different even clear ocean water is from pure sea water. Note that natural water ranges from absorption-dominated ($\omega_0 = 0.247$) to scattering-dominated ($\omega_0 = 0.833$) at $\lambda = 514$ nm. The ratio of backscattering to total scattering is typically a few percent in natural water. However, there is no clear relation between $b_b/b$ and the water type, at least for the Petzold data of Table 13. This lack of an obvious relation is likely the result of differing particle types in the three waters. Since refraction and reflection are important processes at large scattering angles, the particle indices of refraction are important in determining $b_b$. Total scattering is dominated by diffraction and so particle composition has little effect on $b$ values. The last row of Table 13 gives the angle $\psi$ such that one-half of the total scattering occurs at angles between 0 and $\psi$. This angle is rarely greater than 10° in natural waters.

## 43.19 WAVELENGTH DEPENDENCE OF SCATTERING: BIO-OPTICAL MODELS

The strong $\lambda^{-4.32}$ wavelength dependence of pure-water scattering is not seen in natural waters. This is because scattering is dominated by diffraction from polydisperse particles that are usually much larger than the wavelength of visible light. Although diffraction depends on the particle size-to-wavelength ratio, the presence of particles of many sizes

**TABLE 12** Volume Scattering Functions $\beta(\psi, \lambda)$ for Three Oceanic Waters and for Pure Sea Water and a Typical Particle Phase Function $\tilde{\beta}_p(\psi, \lambda)$, All at $\lambda = 514$ nm

| Scattering angle (deg) | Volume scattering functions ($m^{-1}\,sr^{-1}$) | | | | Particle phase function‡ ($sr^{-1}$) |
|---|---|---|---|---|---|
| | Clear ocean* | Coastal ocean* | Turbid harbor* | Pure sea water† | |
| 0.100 | $5.318 \times 10^{1}$ | $6.533 \times 10^{2}$ | $3.262 \times 10^{3}$ | $2.936 \times 10^{-4}$ | $1.767 \times 10^{3}$ |
| 0.126 | 4.042 | 4.577 | 2.397 | 2.936 | 1.296 |
| 0.158 | 3.073 | 3.206 | 1.757 | 2.936 | $9.502 \times 10^{2}$ |
| 0.200 | 2.374 | 2.252 | 1.275 | 2.936 | 6.991 |
| 0.251 | 1.814 | 1.579 | $9.260 \times 10^{2}$ | 2.936 | 5.140 |
| 0.316 | 1.360 | 1.104 | 6.764 | 2.936 | 3.764 |
| 0.398 | $9.954 \times 10$ | $7.731 \times 10^{1}$ | 5.027 | 2.936 | 2.763 |
| 0.501 | 7.179 | 5.371 | 3.705 | 2.936 | 2.012 |
| 0.631 | 5.110 | 3.675 | 2.676 | 2.936 | 1.444 |
| 0.794 | 3.591 | 2.481 | 1.897 | 2.936 | 1.022 |
| 1.000 | 2.498 | 1.662 | 1.329 | 2.936 | $7.161 \times 10^{1}$ |
| 1.259 | 1.719 | 1.106 | $9.191 \times 10^{1}$ | 2.935 | 4.958 |
| 1.585 | 1.171 | $7.306 \times 10^{0}$ | 6.280 | 2.935 | 3.395 |
| 1.995 | $7.758 \times 10^{-1}$ | 4.751 | 4.171 | 2.934 | 2.281 |
| 2.512 | 5.087 | 3.067 | 2.737 | 2.933 | 1.516 |
| 3.162 | 3.340 | 1.977 | 1.793 | 2.932 | 1.002 |
| 3.981 | 2.196 | 1.273 | 1.172 | 2.930 | $6.580 \times 10^{0}$ |
| 5.012 | 1.446 | $8.183 \times 10^{-1}$ | $7.655 \times 10^{0}$ | 2.926 | 4.295 |
| 6.310 | $9.522 \times 10^{-2}$ | 5.285 | 5.039 | 2.920 | 2.807 |
| 7.943 | 6.282 | 3.402 | 3.302 | 2.911 | 1.819 |
| 10.0 | 4.162 | 2.155 | 2.111 | 2.896 | 1.153 |
| 15.0 | 2.038 | $9.283 \times 10^{-2}$ | $9.041 \times 10^{-1}$ | 2.847 | $4.893 \times 10^{-1}$ |
| 20.0 | 1.099 | 4.427 | 4.452 | 2.780 | 2.444 |
| 25.0 | $6.166 \times 10^{-3}$ | 2.390 | 2.734 | 2.697 | 1.472 |
| 30.0 | 3.888 | 1.445 | 1.613 | 2.602 | $8.609 \times 10^{-2}$ |
| 35.0 | 2.680 | $9.063 \times 10^{-3}$ | 1.109 | 2.497 | 5.931 |
| 40.0 | 1.899 | 6.014 | $7.913 \times 10^{-2}$ | 2.384 | 4.210 |
| 45.0 | 1.372 | 4.144 | 5.858 | 2.268 | 3.067 |
| 50.0 | 1.020 | 2.993 | 4.388 | 2.152 | 2.275 |
| 55.0 | $7.683 \times 10^{-4}$ | 2.253 | 3.288 | 2.040 | 1.699 |
| 60.0 | 6.028 | 1.737 | 2.548 | 1.934 | 1.313 |
| 65.0 | 4.883 | 1.369 | 2.041 | 1.839 | 1.046 |
| 70.0 | 4.069 | 1.094 | 1.655 | 1.756 | $8.488 \times 10^{-3}$ |
| 75.0 | 3.457 | $8.782 \times 10^{-4}$ | 1.345 | 1.690 | 6.976 |
| 80.0 | 3.019 | 7.238 | 1.124 | 1.640 | 5.842 |
| 85.0 | 2.681 | 6.036 | $9.637 \times 10^{-3}$ | 1.610 | 4.953 |
| 90.0 | 2.459 | 5.241 | 8.411 | 1.600 | 4.292 |
| 95.0 | 2.315 | 4.703 | 7.396 | 1.610 | 3.782 |
| 100.0 | 2.239 | 4.363 | 6.694 | 1.640 | 3.404 |
| 105.0 | 2.225 | 4.189 | 6.220 | 1.690 | 3.116 |
| 110.0 | 2.239 | 4.073 | 5.891 | 1.756 | 2.912 |
| 115.0 | 2.265 | 3.994 | 5.729 | 1.839 | 2.797 |
| 120.0 | 2.339 | 3.972 | 5.549 | 1.934 | 2.686 |
| 125.0 | 2.505 | 3.984 | 5.343 | 2.040 | 2.571 |
| 130.0 | 2.629 | 4.071 | 5.154 | 2.152 | 2.476 |
| 135.0 | 2.662 | 4.219 | 4.967 | 2.268 | 2.377 |
| 140.0 | 2.749 | 4.458 | 4.822 | 2.384 | 2.329 |
| 145.0 | 2.896 | 4.775 | 4.635 | 2.497 | 2.313 |
| 150.0 | 3.088 | 5.232 | 4.634 | 2.602 | 2.365 |
| 155.0 | 3.304 | 5.824 | 4.900 | 2.697 | 2.506 |
| 160.0 | 3.627 | 6.665 | 5.142 | 2.780 | 2.662 |
| 165.0 | 4.073 | 7.823 | 5.359 | 2.847 | 2.835 |
| 170.0 | 4.671 | 9.393 | 5.550 | 2.896 | 3.031 |
| 175.0 | 4.845 | 9.847 | 5.618 | 2.926 | 3.092 |
| 180.0 | 5.109 | $1.030 \times 10^{-3}$ | 5.686 | 2.936 | 3.154 |

* Data reproduced from Petzold.[53]
† Computed from Eq. (2) and Table 10.
‡ Courtesy of H. R. Gordon; see also Ref. 62.

**TABLE 13** Selected Inherent Optical Properties for the Waters Presented in Fig. 12 and in Table 12 (All values are for $\lambda = 514$ nm except as noted.)

| Water | $a$ ($m^{-1}$) | $b$ ($m^{-1}$) | $c$ ($m^{-1}$) | $\omega_0$ | $b_b/b$ | $\psi$ for $\frac{1}{2}b$ (deg) |
|---|---|---|---|---|---|---|
| Pure sea water | 0.0405* | 0.0025† | 0.043 | 0.058 | 0.500 | 90.00 |
| Clear ocean | 0.114‡ | 0.037 | 0.151§ | 0.247 | 0.044 | 6.25 |
| Coastal ocean | 0.179‡ | 0.219 | 0.398§ | 0.551 | 0.013 | 2.53 |
| Turbid harbor | 0.366‡ | 1.824 | 2.190§ | 0.833 | 0.020 | 4.68 |

* Value obtained by interpolation in Table 6.
† Value obtained by interpolation in Table 10.
‡ Estimated by Petzold[53] from $c(530\text{ nm}) - b(514\text{ nm})$.
§ Measured by Petzold[53] at $\lambda = 530$ nm.

diminishes the wavelength effects that are seen in diffraction by a single particle. Moreover, diffraction does not depend on particle composition. However, some wavelength dependence is to be expected, especially at backward scattering angles where refraction, and hence particle composition, is important. Molecular scattering also contributes something to the total scattering and can even dominate the particle contribution at backscatter angles in clear water.[63]

Morel[64] presents several useful observations on the wavelength dependence of scattering. Figure 13 shows two sets of volume scattering functions, one from the very clear waters of the Tyrrhenian Sea and one from the turbid English Channel. Each set displays $\beta(\psi, \lambda)/\beta(90°, \lambda)$ for $\lambda = 366$, 436, and 546 nm. The clear water shows a definite dependence of the shape of $\beta(\psi, \lambda)$ on $\lambda$ whereas the particle-rich turbid water shows much less wavelength dependence. In each case the volume scattering function of shortest

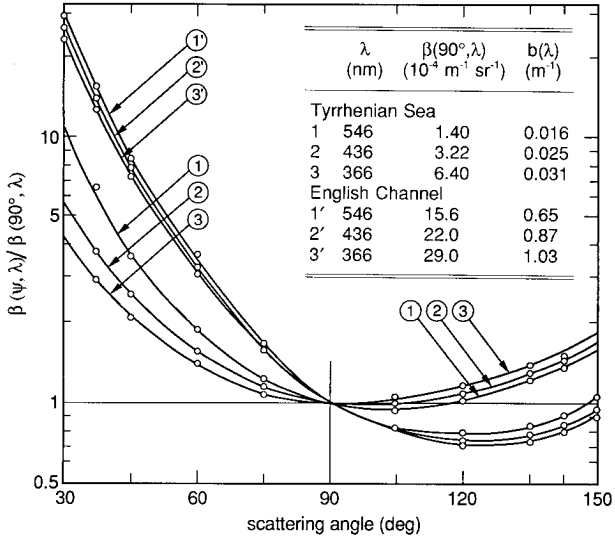


**FIGURE 13** Wavelength dependence of total volume scattering functions measured in very clear (Tyrrhenian Sea) and in turbid (English Channel) waters. (*Redrawn from Morel.*[64])

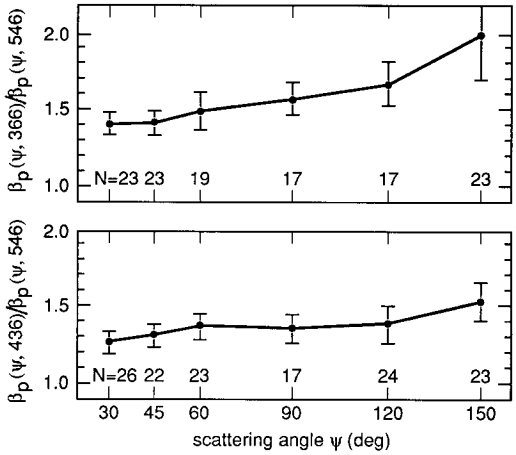


**FIGURE 14** Wavelength dependence of particulate volume scattering functions. $N$ is the number of samples. (*Redrawn from Morel.*[64])

wavelength is most nearly symmetric about $\psi = 90°$, presumably because symmetric molecular scattering is contributing relatively more to the total scattering at short wavelengths.

Figure 14 shows a systematic wavelength dependence of particle volume scattering functions. Figure 14*a* shows average values of $\beta_p(\psi, 366\text{ nm})/\beta_p(\psi, 546\text{ nm})$ for $N$ samples as labeled in the figure. The vertical bars are one standard deviation of the observations. Figure 14*b* shows the ratio for $\lambda = 436$ to 546 nm. These ratios clearly depend both on wavelength and scattering angle. Assuming that $\beta_p(\psi, \lambda)$ has a wavelength dependence of

$$\beta_p(\psi, \lambda) = \beta_p(\psi, 546)\left(\frac{546\text{ nm}}{\lambda}\right)^n$$

the data of Fig. 14 imply values for $n$ as seen in Table 14. As anticipated, the wavelength dependence is strongest for backscatter ($\psi = 150°$) and weakest for forward scatter ($\psi = 30°$).

Kopelevich[49,65] has statistically derived a two-parameter model for spectral volume scattering functions (VSFs). This model separates the contributions by "small" and "large" particles to the particulate scattering. Small particles are taken to be mineral particles less than 1 μm in size and having an index of refraction of $n = 1.15$; large particles are biologic

**TABLE 14** Exponents $n$ Required to Fit the Data of Fig. 14 Assuming That $\beta_p(\psi, \lambda) = \beta_p(\psi, 546)(546/\lambda)^n$

| Wavelength $\lambda$ (nm) | Scattering angle $\psi$ | | |
|---|---|---|---|
| | 30° | 90° | 150° |
| 366 | 0.84 | 1.13 | 1.73 |
| 436 | 0.99 | 1.33 | 1.89 |

particles larger than 1 μm in size and having an index refraction of $n = 1.03$. The model is defined by

$$\beta(\psi, \lambda) = \beta_w(\psi, \lambda) + v_s\beta_s^*(\psi)\left(\frac{550\text{ nm}}{\lambda}\right)^{1.7} + v_\ell\beta_\ell^*(\psi)\left(\frac{550\text{ nm}}{\lambda}\right)^{0.3} \tag{4}$$

with the following definitions:

| | |
|---|---|
| $\beta_w(\psi, \lambda)$ | the VSF of pure sea water, given by Eq. (2) with $\lambda_0 = 550$ nm and an exponent of 4.30 |
| $v_s$ | the volume concentration of small particles, with units of $cm^3$ of particles per $m^3$ of water, i.e., parts per million (ppm) |
| $v_\ell$ | the analogous volume concentration of large particles |
| $\beta_s^*(\psi)$ | the small-particle VSF per unit volume concentration of small particles, with units of $m^{-1}\,sr^{-1}\,ppm^{-1}$ |
| $\beta_\ell^*(\psi)$ | the analogous large-particle concentration-specific VSF |

The concentration-specific VSFs for small and large particles are given in Table 15. Equation (4) can be evaluated as if the two parameters $v_s$ and $v_\ell$ are known; the ranges of values for oceanic waters are $0.01 \le v_s \le 0.20$ ppm and $0.01 \le v_\ell \le 0.40$ ppm. However, these two parameters are themselves parametrized in terms of the total volume scattering function measured at $\lambda = 550$ nm for $\psi = 1$ and 45°:

$$\begin{aligned} v_s &= -1.4 \times 10^{-4}\beta(1°, 550\text{ nm}) + 10.2\beta(45°, 550\text{ nm}) - 0.002 \\ v_\ell &= 2.2 \times 10^{-2}\beta(1°, 550\text{ nm}) - 1.2\beta(45°, 550\text{ nm}) \end{aligned} \tag{5}$$

Thus $\beta(\psi, \lambda)$ can also be determined from two measurements of the total VSF.

The mathematical form of the Kopelevich model reveals its underlying physics. Large particles give diffractive scattering at very small angles; thus $\beta_\ell^*(\psi)$ is highly peaked for small $\psi$ and the wavelength dependence of the large particle term is weak ($\lambda^{-0.3}$). Small

**TABLE 15** The Concentration-Specific Volume Scattering Functions for Small ($\beta_s^*$) and Large ($\beta_\ell^*$) Particles As a Function of the Scattering Angle $\psi$ for Use in the Kopelevich Model for Spectral Volume Scattering Functions, Eq. (4)*

| $\psi$ (deg) | $\beta_s^*$ $\left(\frac{m^{-1}\,sr^{-1}}{ppm}\right)$ | $\beta_\ell^*$ $\left(\frac{m^{-1}\,sr^{-1}}{ppm}\right)$ | $\psi$ (deg) | $\beta_s^*$ $\left(\frac{m^{-1}\,sr^{-1}}{ppm}\right)$ | $\beta_\ell^*$ $\left(\frac{m^{-1}\,sr^{-1}}{ppm}\right)$ |
|---|---|---|---|---|---|
| 0 | 5.3 | 140 | 45 | $9.8 \times 10^{-2}$ | $6.2 \times 10^{-4}$ |
| 0.5 | 5.3 | 98 | 60 | 4.1 | 3.8 |
| 1 | 5.2 | 46 | 75 | 2.0 | 2.0 |
| 1.5 | 5.2 | 26 | 90 | 1.2 | $6.3 \times 10^{-5}$ |
| 2 | 5.1 | 15 | 105 | $8.6 \times 10^{-3}$ | 4.4 |
| 4 | 4.6 | 3.6 | 120 | 7.4 | 2.9 |
| 6 | 3.9 | 1.1 | 135 | 7.4 | 2.0 |
| 10 | 2.5 | 0.20 | 150 | 7.5 | 2.0 |
| 15 | 1.3 | $5.0 \times 10^{-2}$ | 180 | 8.1 | 7.0 |
| 30 | 0.29 | $2.8 \times 10^{-3}$ | $b^* =$ | $1.34\ m^{-1}$/ppm | $0.312\ m^{-1}$/ppm |

* Reproduced from Kopelevich.[49]

particles contribute more to scattering at large angles and thus have a more symmetric VSF and a stronger wavelength dependence ($\lambda^{-1.7}$). This model gives a reasonably good description of VSFs observed in a variety of waters (Shifrin,[58] fig. 5.20).

Several simple models are available for the scattering coefficient $b(\lambda)$. A commonly employed bio-optical model for $b(\lambda)$ is that of Gordon and Morel[66] (see also Ref. 6):

$$b(\lambda) = b_w(\lambda) + \left(\frac{550\text{ nm}}{\lambda}\right)0.30C^{0.62} \qquad \text{m}^{-1} \tag{6}$$

Here $b_w(\lambda)$ is given by Eq. (3) and Table 10. $\lambda$ is in nm and $C$ is the chlorophyll concentration in mg m$^{-3}$. A related bio-optical model for the backscatter coefficient $b_b(\lambda)$ is found in Morel[45]:

$$b_b(\lambda) = \tfrac{1}{2}b_w(\lambda) + \left[0.002 + 0.02(\tfrac{1}{2} - \tfrac{1}{4}\log C)\left(\frac{550\text{ nm}}{\lambda}\right)\right]0.30C^{0.62}$$

The $(\frac{1}{2} - \frac{1}{4}\log C)$ factor gives $b_b(\lambda)$ a $\lambda^{-1}$ wavelength dependence in very clear ($C = 0.01$ mg m$^{-1}$) water and no wavelength dependence in very turbid ($C = 100$ mg m$^{-3}$) water. These empirically derived models are intended for use only in case 1 waters.

A feeling for the accuracy of the $b(\lambda)$ model of Eq. (6) can be obtained from Fig. 15, which plots measured $b(550\text{ nm})$ values versus chlorophyll concentration $C$ in both case 1 and case 2 waters. Note that even when the model is applied to the case 1 waters from which it was derived, the predicated $b(550\text{ nm})$ value easily can be wrong by a factor of 2. If the model is misapplied to case 2 waters, the error can be an order of magnitude. Note that for a given $C$ value, $b(550\text{ nm})$ is higher in case 2 waters than in case 1 waters, presumably because of the presence of additional particles that do not contain chlorophyll.

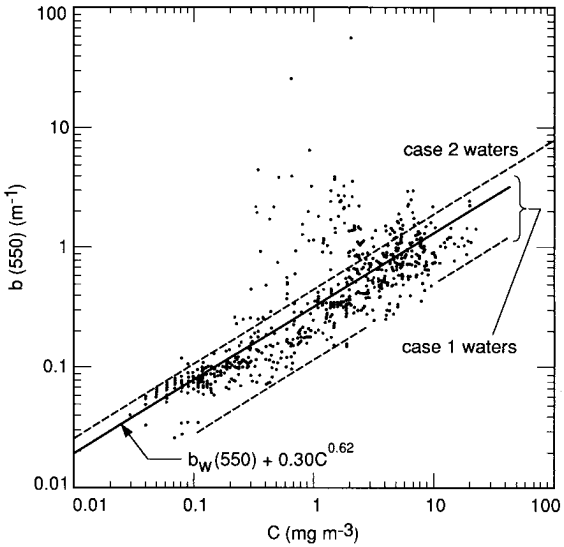


**FIGURE 15** Measured scattering coefficients at $\lambda = 550$ nm, $b(550)$, as a function of chlorophyll concentration $C$. Case 1 waters lie between the dashed lines. Case 2 waters lie above the upper dashed line, which is defined by $b(550) = 0.45C^{0.62}$. The solid line is the model of Eq. (6). (*Redrawn from Gordon and Morel,*[66] *with permission.*)

Integration over $\psi$ of the Kopelevich $b(\psi, \lambda)$ model of Eq. (4) yields another model for $b(\lambda)$:

$$b(\lambda) = 0.0017\left(\frac{550\text{ nm}}{\lambda}\right)^{4.3} + 1.34v_s\left(\frac{550\text{ nm}}{\lambda}\right)^{1.7} + 0.312v_\ell\left(\frac{550\text{ nm}}{\lambda}\right)^{0.3} \qquad \text{m}^{-1}$$

where $v_s$ and $v_\ell$ are given by Eq. (5). Kopelevich claims that the accuracy of this model is ~30 percent.

A bio-optical model related to the Kopelevich model is found in Haltrin and Kattawar[50] (their notation):

$$b(\lambda) = b_w(\lambda) + b^0_{ps}(\lambda)P_s + b^0_{p\ell}(\lambda)P_\ell$$

Here $b_w(\lambda)$ is given by

$$b_w(\lambda) = 5.826 \times 10^{-3}\left(\frac{400}{\lambda}\right)^{4.322}$$

which is essentially the same as Eq. (3) and the data in Table 10. The terms $b^0_{ps}(\lambda)$ and $b^0_{p\ell}(\lambda)$ are the specific scattering coefficients for small and large particles, respectively, and are given by

$$b^0_{ps}(\lambda) = 1.1513\left(\frac{400}{\lambda}\right)^{1.7} \qquad \text{m}^2\,\text{g}^{-1}$$

$$b^0_{p\ell}(\lambda) = 0.3411\left(\frac{400}{\lambda}\right)^{0.3} \qquad \text{m}^2\,\text{g}^{-1}$$

$P_s$ and $P_\ell$ are the concentrations in $\text{g m}^{-3}$ of small and large particles, respectively. These quantities are parametrized in terms of the chlorophyll concentration $C$, as shown in Table 16. This work also presents a model for backscattering:

$$b_b(\lambda) = \tfrac{1}{2}b_w(\lambda) + B_s b^0_{ps}(\lambda)P_s + B_\ell b^0_{p\ell}(\lambda)\text{P}_\ell$$

Here $B_s = 0.039$ is the backscattering probability for small particles and $B_\ell = 0.00064$ is the backscattering probability for large particles.

The bio-optical models for scattering just discussed are useful but very approximate.

**TABLE 16** Parameterization of Small ($P_s$) and Large ($P_\ell$) Particle Concentrations in Terms of the Chlorophyll Concentration $C$ for use in the Kopelevich-Haltrin-Kattawar Models for $b(\lambda)$ and $b_b(\lambda)$*

| $C$ ($\text{mg m}^{-3}$) | $P_s$ ($\text{g m}^{-3}$) | $P_\ell$ ($\text{g m}^{-3}$) |
|---|---|---|
| 0.00 | 0.000 | 0.000 |
| 0.03 | 0.001 | 0.035 |
| 0.05 | 0.002 | 0.051 |
| 0.12 | 0.004 | 0.098 |
| 0.30 | 0.009 | 0.194 |
| 0.60 | 0.016 | 0.325 |
| 1.00 | 0.024 | 0.476 |
| 3.00 | 0.062 | 1.078 |

* Reproduced from Haltrin and Kattawar,[50] with permission.

The reason for the frequent large discrepancies between model predictions and measured reality likely lies in the fact that scattering depends not just on particle concentration (as parameterized in terms of chlorophyll concentration), but also on the particle index of refraction and on the details of the particle size distribution which are not well parameterized in terms of the chlorophyll concentration alone. Whether or not the Kopelevich model or its derivative Haltrin-Kattawar form which partition the scattering into large and small particle components is in some sense better than the Gordon-Morel model is not known at present. Another consequence of the complexity of scattering is seen in the next section.

## 43.20 BEAM ATTENUATION

The spectral beam attenuation coefficient $c(\lambda)$ is just the sum of the spectral absorption and scattering coefficients: $c(\lambda) = a(\lambda) + b(\lambda)$. Since both $a(\lambda)$ and $b(\lambda)$ are highly variable functions of the nature and concentration of the constituents of natural waters so is $c(\lambda)$. Beam attenuation near $\lambda = 660$ nm is the only inherent optical property of water that is easily, accurately, and routinely measured. This wavelength is used both for engineering reasons (the availability of a stable LED light source) and because absorption by yellow matter is negligible in the red. Thus the quantity

$$c_p(660\text{ nm}) \equiv c(660\text{ nm}) - a_w(660\text{ nm}) - b_w(660\text{ nm}) \equiv c(660\text{ nm}) - c_w(660\text{ nm})$$

is determined by the nature of the suspended particulate matter. The particulate beam attenuation $c_p(660\text{ nm})$ is highly correlated with total particle volume concentration (usually expressed in parts per million), but it is much less well correlated with chlorophyll concentration.[67] The particulate beam attenuation can be used to estimate the total particulate load (often expressed as $\text{g m}^{-3}$).[68] However, the dependence of the particulate beam attenuation on particle properties is not simple. Spinrad[69] used Mie theory to calculate the dependence of the volume-specific particulate beam attenuation (particulate beam attenuation coefficient $c_p$ in $\text{m}^{-1}$ per unit suspended particulate volume in parts per million) on the relative refractive index and on the slope $s$ of an assumed Junge size distribution for particles in the size range 1–80 μm; the result is shown in Fig. 16.

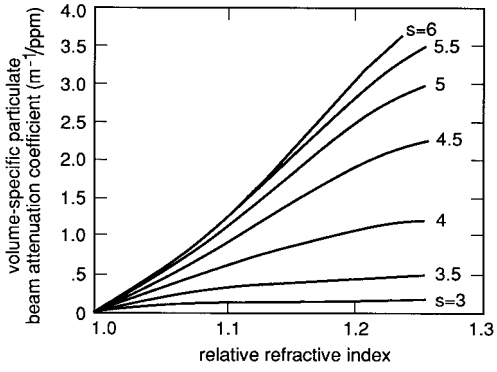


**FIGURE 16** Computed relationship between volume-specific particulate beam attenuation coefficient, relative refractive index, and slope $s$ of a Junge number size distribution. (*Reproduced from Spinrad,*[69] *with permission.*)

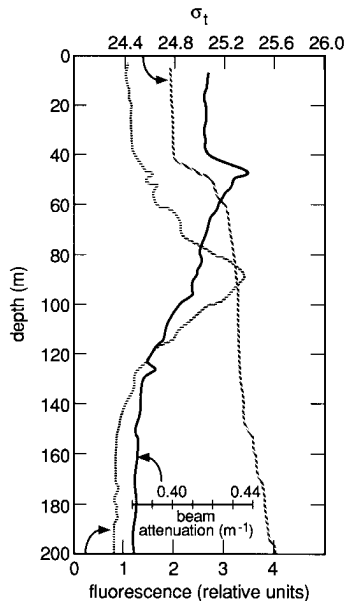


**FIGURE 17** Example from the Pacific Ocean water of the depth dependence of beam attenuation (solid line), water density ($\sigma_t$, dashed line), and chlorophyll concentration (fluorescence, dotted line). (*Reproduced from Kitchen and Zaneveld,*[70] *with permission.*)

Although the details of the figure are sensitive to the choice of upper and lower size limits in the Mie calculations, the qualitative behavior of the curves is generally valid and supports the statements made in the closing paragraph of Sec. 43.19.

Because of the complicated dependence of scattering and hence of beam attenuation on particle properties, the construction of bio-optical models for $c(\lambda)$ is not easy. The reason is that chlorophyll concentration alone is not sufficient to parametrize scattering.[70] Figure 17 illustrates this insufficiency. The figure plots vertical profiles of $c(665\text{ nm})$, water density (proportional to the oceanographic variable $\sigma_t$), and chlorophyll concentration (proportional to fluorescence by chlorophyll and related pigments). Note that the maximum in beam attenuation at 46 m depth coincides with the interface (pycnocline) between less dense water above and more dense water below. Peaks in beam attenuation are commonly observed at density interfaces because particle concentrations are often greatest there. The maximum in chlorophyll concentration occurs at a depth of 87 m. The chlorophyll concentration depends not just on the number or volume of chlorophyll-bearing particles but also on their photoadaptive state, which depends on nutrient availability and ambient lighting. Thus chlorophyll concentration cannot be expected to correlate well with total scattering or with particulate beam attenuation $c_p(\lambda)$.

Voss[71] has developed an empirical model for $c(\lambda)$ given a measurement of $c$ at $\lambda = 490\text{ nm}$:

$$c(\lambda) = c_w(\lambda) + [c(490\text{ nm}) - c_w(490\text{ nm})][1.563 - 1.149 \times 10^{-3}\lambda]$$

where $\lambda$ is in nm and $c$ is in $m^{-1}$. The attenuation coefficient for pure sea water, $c_w = a_w + b_w$, is given by the Smith-Baker data of Table 6. This model was statistically

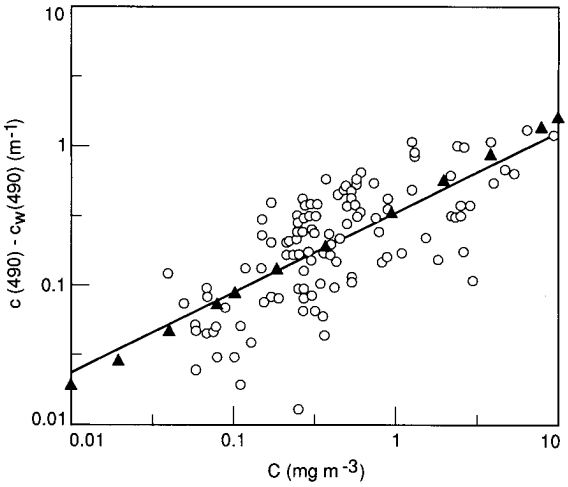


**FIGURE 18** Particulate beam attenuation at 490 nm (open circles) as a function of chlorophyll concentration $C$ as used to determine Eq. (7) which is given by the solid line. Solid triangles give values as predicted by the sum of Eqs. (1) and (6). (*Redrawn from Voss,*[71] *with permission.*)

derived from data of global extent. Testing of the model with independent data usually gave errors of less than 5 percent, although occasional errors of ~20 percent were found.

Voss also determined a least-squares fit of $c(490)$ to the chlorophyll concentration. The result

$$c(490\text{ nm}) = 0.39C^{0.57} \tag{7}$$

is similar in form to the chlorophyll dependence of the $a(\lambda)$ and $b(\lambda)$ models seen in Eqs. (1) and (6), respectively. Figure 18 shows the spread of the data points used to determine Eq. (7). Note that for a given value of $C$ there is an order-of-magnitude spread in values of $c(490\text{ nm})$. The user of Eq. (7) or of the models for $b(\lambda)$ must always keep in mind that large deviations from the predicted values will be found in natural waters.

## 43.21 DIFFUSE ATTENUATION AND JERLOV WATER TYPES

As seen in Fig. 1 and in Table 1 there is a so-called diffuse attenuation coefficient for any radiometric variable. The most commonly used diffuse attenuation coefficients are those for downwelling plane irradiance, $K_d(z, \lambda)$, and for PAR, $K_{PAR}(z)$. Although the various diffuse attenuation coefficients are conceptually distinct, in practice they are often numerically similar and they all asymptotically approach a common value at great depths in homogeneous water.[2] The monograph by Tyler and Smith[72] gives tabulations and plots of $E_d(z, \lambda)$, $E_u(z, \lambda)$ and the associated $K_d(z, \lambda)$, $K_u(z, \lambda)$ and $R(z, \lambda)$ measured in a variety of waters.

Observation shows that $K_d(z, \lambda)$ varies systematically with wavelength over a wide range of waters from very clear to very turbid. Moreover, $K_d(z, \lambda)$ is often rather

insensitive to environmental effects[73] except for extreme conditions[74] (such as the sun within 10° of the horizon) and in most cases correction can be made[11] for the environmental effects that are present in $K_d$. $K_d$ therefore is regarded as a quasi-inherent optical property whose variability is governed primarily by changes in the inherent optical properties of the water body and not by changes in the external environment.

Jerlov[29] exploited this benign behavior of $K_d$ to develop a frequently used classification scheme for oceanic waters based on the spectral shape of $K_d$. The *Jerlov water types* are in essence a classification based on water clarity as quantified by $K_d(z_s, \lambda)$ where $z_s$ is a depth just below the sea surface. This classification scheme can be contrasted with the case 1 and case 2 classification described earlier, which is based on the nature of the suspended matter within the water. The Jerlov water types are numbered I, IA, IB, II, and III for open ocean waters, and 1 through 9 for coastal waters. Type I is the clearest and type III is the most turbid open ocean water. Likewise, for coastal waters type 1 is clearest and type 9 is most turbid. The Jerlov types I–III generally correspond to case 1 water since phytoplankton predominate in the open ocean. Types 1–9 correspond to case 2 waters where yellow matter and terrigenous particulates dominate the optical properties. A rough correspondence between chlorophyll concentration and Jerlov oceanic water type is given by[45]

$$\begin{array}{ll} C: & 0\text{–}0.01 \sim 0.05 \sim 0.1 \sim 0.5 \sim 1.5\text{–}2.0\ \mathrm{mg\ m^{-3}} \\ \text{water type:} & \quad \mathrm{I} \quad \mathrm{IA} \quad \mathrm{IB} \quad \mathrm{II} \quad \mathrm{III} \end{array}$$

Austin and Petzold[75] reevaluated the Jerlov classification using an expanded database and slightly revised the $K_d(\lambda)$ values used by Jerlov in his original definition of the water types. Table 17 gives the revised values for $K_d(\lambda)$ for the water types commonly encountered in oceanography. These values are recommended over those found in

**TABLE 17** Downwelling Irradiance Diffuse Attenuation Coefficients $K_d(\lambda)$ Used to Define the Jerlov Water Types As Determined by Austin and Petzold* (All quantities in the body of the Table have units of $m^{-1}$.)

| $\lambda$ (nm) | Jerlov water type | | | | | |
|---|---|---|---|---|---|---|
| | I | IA | IB | II | III | 1 |
| 350 | 0.0510 | 0.0632 | 0.0782 | 0.1325 | 0.2335 | 0.3345 |
| 375 | 0.0302 | 0.0412 | 0.0546 | 0.1031 | 0.1935 | 0.2839 |
| 400 | 0.0217 | 0.0316 | 0.0438 | 0.0878 | 0.1697 | 0.2516 |
| 425 | 0.0185 | 0.0280 | 0.0395 | 0.0814 | 0.1594 | 0.2374 |
| 450 | 0.0176 | 0.0257 | 0.0355 | 0.0714 | 0.1381 | 0.2048 |
| 475 | 0.0184 | 0.0250 | 0.0330 | 0.0620 | 0.1160 | 0.1700 |
| 500 | 0.0280 | 0.0332 | 0.0396 | 0.0627 | 0.1056 | 0.1486 |
| 525 | 0.0504 | 0.0545 | 0.0596 | 0.0779 | 0.1120 | 0.1461 |
| 550 | 0.0640 | 0.0674 | 0.0715 | 0.0863 | 0.1139 | 0.1415 |
| 575 | 0.0931 | 0.0960 | 0.0995 | 0.1122 | 0.1359 | 0.1596 |
| 600 | 0.2408 | 0.2437 | 0.2471 | 0.2595 | 0.2826 | 0.3057 |
| 625 | 0.3174 | 0.3206 | 0.3245 | 0.3389 | 0.3655 | 0.3922 |
| 650 | 0.3559 | 0.3601 | 0.3652 | 0.3837 | 0.4181 | 0.4525 |
| 675 | 0.4372 | 0.4410 | 0.4457 | 0.4626 | 0.4942 | 0.5257 |
| 700 | 0.6513 | 0.6530 | 0.6550 | 0.6623 | 0.6760 | 0.6896 |

* Reproduced from Austin and Petzold[75] with permission.

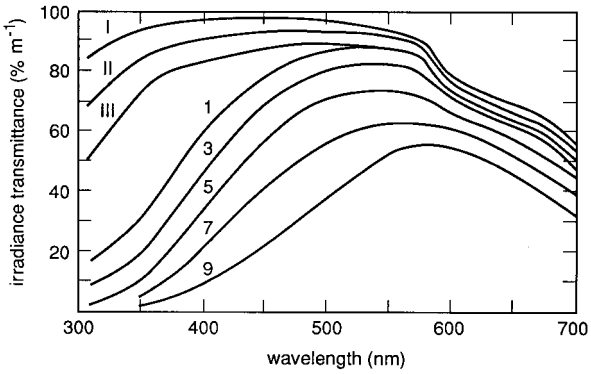


**FIGURE 19** Percentage transmittance per meter of water of downwelling irradiance $E_d$ as a function of wavelength for selected Jerlov water types. (*Reproduced from Jerlov,*[29] with permission.)

Jerlov.[29] Figure 19 shows the percent transmittance of $E_d(\lambda)$ per meter of water for selected Jerlov water types. Note how the wavelength of maximum transmittance shifts from blue in the clearest open ocean water (type I) to green (types III and 1) to yellow in the most turbid, yellow-matter-rich coastal water (type 9).

Austin and Petzold also presented a simple model that allows the determination of $K_d(\lambda)$ at all wavelengths from a value of $K_d$ measured at any single wavelength. This model is defined by

$$K_d(\lambda) = \frac{M(\lambda)}{M(\lambda_0)}[K_d(\lambda_0) - K_{dw}(\lambda_0)] + K_{dw}(\lambda)$$

Here $\lambda_0$ is the wavelength at which $K_d$ is measured and $K_{dw}$ refers to values for pure sea water. $K_{dw}(\lambda)$ and the statistically derived coefficients $M(\lambda)$ are given in Table 18. (These

**TABLE 18** Values of the Coefficient $M(\lambda)$ and of the Downwelling Diffuse Attenuation Coefficient for Pure Sea Water, $K_{dw}(\lambda)$, for Use in the Austin and Petzold Model for $K_d(\lambda)$*

| $\lambda$ (nm) | $M$ ($m^{-1}$) | $K_{dw}$ ($m^{-1}$) | $\lambda$ (nm) | $M$ ($m^{-1}$) | $K_{dw}$ ($m^{-1}$) | $\lambda$ (nm) | $M$ ($m^{-1}$) | $K_{dw}$ ($m^{-1}$) |
|---|---|---|---|---|---|---|---|---|
| 350 | 2.1442 | 0.0510 | 470 | 1.1982 | 0.0179 | 590 | 0.4840 | 0.1578 |
| 360 | 2.0504 | 0.0405 | 480 | 1.0955 | 0.0193 | 600 | 0.4903 | 0.2409 |
| 370 | 1.9610 | 0.0331 | 490 | 1.0000 | 0.0224 | 610 | 0.5090 | 0.2892 |
| 380 | 1.8772 | 0.0278 | 500 | 0.9118 | 0.0280 | 620 | 0.5380 | 0.3124 |
| 390 | 1.8009 | 0.0242 | 510 | 0.8310 | 0.0369 | 630 | 0.6231 | 0.3296 |
| 400 | 1.7383 | 0.0217 | 520 | 0.7578 | 0.0498 | 640 | 0.7001 | 0.3290 |
| 410 | 1.7591 | 0.0200 | 530 | 0.6924 | 0.0526 | 540 | 0.7300 | 0.3559 |
| 420 | 1.6974 | 0.0189 | 540 | 0.6350 | 0.0577 | 660 | 0.7301 | 0.4105 |
| 430 | 1.6108 | 0.0182 | 550 | 0.5860 | 0.0640 | 670 | 0.7008 | 0.4278 |
| 440 | 1.5169 | 0.0178 | 560 | 0.5457 | 0.0723 | 680 | 0.6245 | 0.4521 |
| 450 | 1.4158 | 0.0176 | 570 | 0.5146 | 0.0842 | 690 | 0.4901 | 0.5116 |
| 460 | 1.3077 | 0.0176 | 580 | 0.4935 | 1.1065 | 700 | 0.2891 | 0.6514 |

* Condensed with permission from Austin and Petzold,[75] who give values every 5 nm.

$K_{dw}$ values differ slightly from those seen in Table 6.) This model is valid in waters where $K_d(490) \leq 0.16\ m^{-1}$ which corresponds to a chlorophyll concentration of $C \leq 3\ mg\ m^{-3}$.

Unlike the beam attenuation coefficient $c(\lambda)$, the diffuse attenuation $K_d(z, \lambda)$ is highly correlated with chlorophyll concentration. The reason is seen in the approximate formula[11]

$$K_d(\lambda) \approx \frac{a(\lambda) + b_b(\lambda)}{\cos \theta_{sw}}$$

where $\theta_{sw}$ is the solar angle measured within the water. Since $a(\lambda) \gg b_b(\lambda)$ for most waters, $K_d(\lambda)$ is largely determined by the absorption properties of the water, which are fairly well parametrized by the chlorophyll concentration. Beam attenuation on the other hand is proportional to the total scattering which is not well parametrized by chlorophyll concentration. Observations show[76] that the beam attenuation at 660 nm is not in general correlated with diffuse attenuation.

A bio-optical model for $K_d(\lambda)$ is given by Morel[45]:

$$K_d(\lambda) = K_{dw}(\lambda) + \chi(\lambda) C^{e(\lambda)}$$

Here $K_{dw}(\lambda)$ is the diffuse attenuation for pure sea water and $\chi(\lambda)$ and $e(\lambda)$ are statistically derived functions that convert the chlorophyll concentration $C$ in $mg\ m^{-3}$ into $K_d$ values in $m^{-1}$. Table 19 gives the $K_{dw}$, $\chi$ and $e$ values used in the Morel model. This model is applicable to case 1 waters with $C \leq 30\ mg\ m^{-3}$, although the $\chi$ and $e$ values are somewhat uncertain for $\lambda > 650$ nm because of sparse data available for their determination. Some feeling for the accuracy of the Morel $K_d(\lambda)$ model can be obtained from Fig. 20 which shows predicted (the line) and observed $K_d(450)$ values as a function of $C$. Errors can be as large as a factor of 2 in case 1 waters (dots) and can be much larger if the model is misapplied to case 2 waters (open circles). The Morel model allows the determination of $K_d(\lambda)$ if $C$ is measured; the Austin and Petzold model determines $K_d(\lambda)$ from a measurement at one wavelength.

**TABLE 19** Values of the Coefficients $\chi(\lambda)$ and $e(\lambda)$ and of the Downwelling Diffuse Attenuation Coefficient for Pure Sea Water, $K_{dw}(\lambda)$, for Use in the Morel Model for $K_d(\lambda)$*

| $\lambda$ (nm) | $\chi(\lambda)$ | $e(\lambda)$ | $K_{dw}(\lambda)$ ($m^{-1}$) | $\lambda$ (nm) | $\chi(\lambda)$ | $e(\lambda)$ | $K_{dw}(\lambda)$ ($m^{-1}$) |
|---|---|---|---|---|---|---|---|
| 400 | 0.1100 | 0.668 | 0.0209 | 550 | 0.0410 | 0.650 | 0.0640 |
| 410 | 0.1125 | 0.680 | 0.0196 | 560 | 0.0390 | 0.640 | 0.0717 |
| 420 | 0.1126 | 0.693 | 0.0183 | 570 | 0.0360 | 0.623 | 0.0807 |
| 430 | 0.1078 | 0.707 | 0.0171 | 580 | 0.0330 | 0.610 | 0.1070 |
| 440 | 0.1041 | 0.707 | 0.0168 | 590 | 0.0325 | 0.618 | 0.1570 |
| 450 | 0.0971 | 0.701 | 0.0168 | 600 | 0.0340 | 0.626 | 0.2530 |
| 460 | 0.0896 | 0.700 | 0.0173 | 610 | 0.0360 | 0.634 | 0.2960 |
| 470 | 0.0823 | 0.703 | 0.0175 | 620 | 0.0385 | 0.642 | 0.3100 |
| 480 | 0.0746 | 0.703 | 0.0194 | 630 | 0.0420 | 0.653 | 0.3200 |
| 490 | 0.0690 | 0.702 | 0.0217 | 640 | 0.0440 | 0.663 | 0.3300 |
| 500 | 0.0636 | 0.700 | 0.0271 | 650 | 0.0450 | 0.672 | 0.3500 |
| 510 | 0.0578 | 0.690 | 0.0384 | 660 | 0.0475 | 0.682 | 0.4050 |
| 520 | 0.0498 | 0.680 | 0.0490 | 670 | 0.0515 | 0.695 | 0.4300 |
| 530 | 0.0467 | 0.670 | 0.0518 | 680 | 0.0505 | 0.693 | 0.4500 |
| 540 | 0.0440 | 0.660 | 0.0568 | 690 | 0.0390 | 0.640 | 0.5000 |
| | | | | 700 | 0.0300 | 0.600 | 0.6500 |

* Condensed with permission from Morel,[45] who gives values every 5 nm.

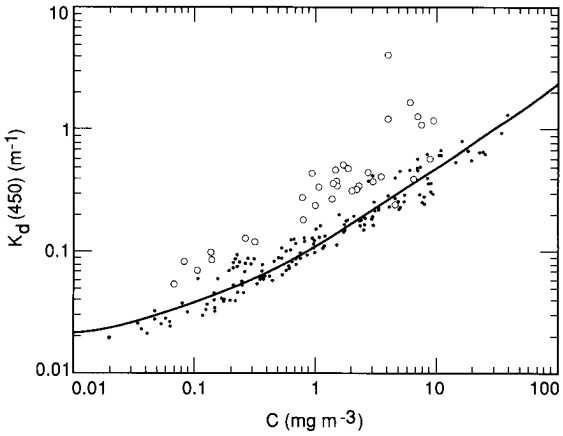


**FIGURE 20** Measured $K_d$ values at 450 nm as a function of chlorophyll concentration $C$. Dots are measurements from case 1 waters; open circles are from case 2 waters. The solid line gives $K_d(450)$ as predicted by the Morel bio-optical model. (*Redrawn from Morel,*[45] *with permission.*)

Morel[45] also presents a very simple bio-optical model for $\bar{K}_{PAR}(0, z_{eu})$ the value of $K_{PAR}(z)$ averaged over the euphotic zone $0 \leq z \leq z_{eu}$:

$$\bar{K}_{PAR}(0, z_{eu}) = 0.121C^{0.428}$$

where $C$ is the mean chlorophyll concentration in the euphotic zone in mg $m^{-3}$ and $\bar{K}_{PAR}$ is in $m^{-1}$. The euphotic zone is the region where there is sufficient light for photosynthesis to take place; it extends roughly to the depth where $E_{PAR}(z)$ is 1 percent of its surface value (i.e., $E_{PAR}(z_{eu}) = 0.01\ E_{PAR}(0)$). Table 20 gives $z_{eu}$ as a function of $C$ as determined by the Morel model.

## 43.22 IRRADIANCE REFLECTANCE AND REMOTE SENSING

The spectral irradiance reflectant $R(\lambda) \equiv E_u(\lambda)/E_d(\lambda)$ is an important apparent optical property. Measurements of $R(z, \lambda)$ within the water have been used[77] to estimate water quality parameters such as the chlorophyll concentration, the particle backscattering coefficient, and the absorption coefficient of yellow matter. More importantly, $R(\lambda)$ just below the water surface can be related to the radiance leaving the water[78]; this radiance is available for detection by aircraft- or satellite-borne instruments. Understanding the dependence of $R(\lambda)$ upon the constituents of natural waters is therefore one of the central problems in remote sensing of water bodies.

Figure 21 illustrates the variability of $R(\lambda)$ in natural waters. Figure 21*a* shows $R(\lambda)$ in percent for various case 1 waters. For low-chlorophyll concentrations $R(\lambda)$ is highest at blue wavelengths, hence the blue color of clean ocean water. As the chlorophyll concentration increases, the maximum in $R(\lambda)$ shifts to green wavelengths. The enhanced reflectance near $\lambda = 685$ nm is due to chlorophyll fluorescence. Also note the exceptionally

**TABLE 20** Approximate Depth of the Euphotic Zone, $z_{eu}$, in Homogeneous Case 1 Water As a Function of Chlorophyll Concentration $C$.*

| $C$ (mg m$^{-3}$) | $z_{eu}$ (m) | $C$ (mg m$^{-3}$) | $z_{eu}$ (m) |
|---|---|---|---|
| 0.0 | 183 | 1 | 39 |
| 0.01 | 153 | 2 | 29 |
| 0.03 | 129 | 3 | 24 |
| 0.05 | 115 | 5 | 19 |
| 0.1 | 95 | 10 | 14 |
| 0.2 | 75 | 20 | 10 |
| 0.3 | 64 | 30 | 8 |
| 0.5 | 52 | | |

* Data extracted from Morel,[45] with permission.

high values measured[20] within a coccolithophore bloom; $R(\lambda)$ is high there because of the strong scattering by the numerous calcite particles (see Sec. 43.6). Figure 21*b* shows $R(\lambda)$ from waters dominated by suspended sediments (i.e., by nonpigmented particles). For high-sediment concentrations $R(\lambda)$ is nearly flat from blue to yellow wavelengths, and therefore the water appears brown. Figure 21*c* is from waters with high concentrations of yellow substances; the peak in $R(\lambda)$ lies in the yellow. With good reason the term ''ocean color'' is often used as a synonym for $R(\lambda)$.

One of the main goals of oceanic remote sensing is the determination of chlorophyll concentrations in near-surface waters because of the fundamental role played by phytoplankton in the global ecosystem. Gordon et al.[78] define the *normalized water-leaving radiance* $[L_w(\lambda)]_N$ as the radiance that would leave the sea surface if the sun were at the zenith and the atmosphere were absent; this quantity is fundamental to remote sensing. They then show that $[L_w]_N$ is directly proportional to $R$ and that $R$ is proportional to $b_b/(a+b_b)$ (i.e., to $b_b/K_d$). Although $a$ or $K_d$ are reasonably well modeled in terms of

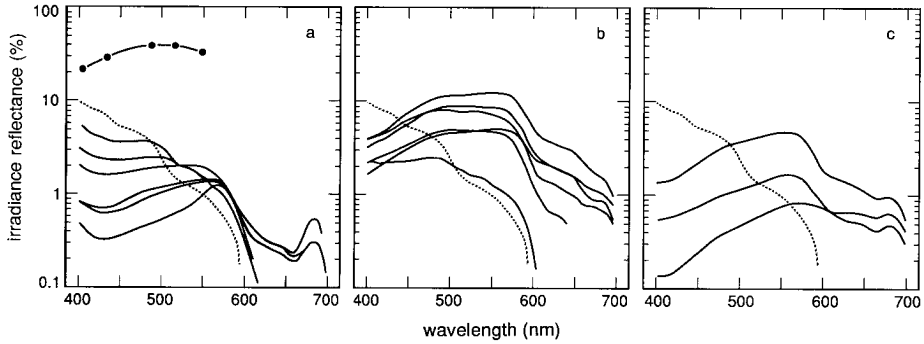


**FIGURE 21** Measured spectral irradiance reflectances $R(\lambda)$ from various waters. Panel (*a*) is from case waters with different quantities of phytoplankton; the dotted line is $R(\lambda)$ for pure sea water. The heavy dots give values measured within a coccolithophore bloom.[20] Panel (*b*) is from case 2 waters dominated by suspended sediments and panel (*c*) is from case 2 waters dominated by yellow matter. (*Redrawn from Sathyendranath and Morel,[79] with permission.*)

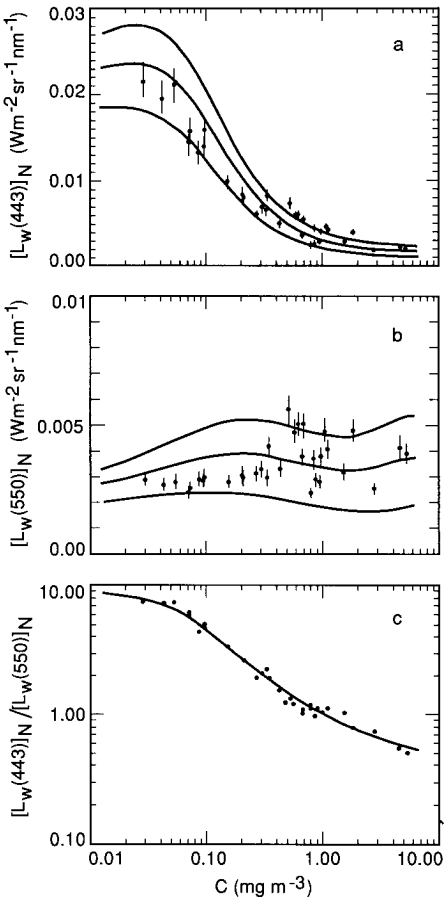


**FIGURE 22** In panels (*a*) and (*b*) the solid lines are values of the normalized water-leaving radiances $[L_w(\lambda)]_N$ at $\lambda = 443$ and 550 nm, respectively, as predicted by various models that relate $[L_w(\lambda)]_N$ to the chlorophyll concentration *C*. The dots are measured values of $[L_w(\lambda)]_N$. Panel (*c*) shows the predicted (line) and observed ratio of the $[L_w(\lambda)]_N$ values of panels (*a*) and (*b*). (*Redrawn from Gordon, et al.,* [78] with permission.)

chlorophyll concentration *C* in case 1 waters, $b_b$ is not well described in terms of *C*. Thus poor agreement is to be expected between observed values of $[L_w(\lambda)]_N$ and values predicted by a model parametrized in terms of *C*. This is indeed the case as is seen in Fig. 22*a* and *b* which shows observed and predicted $[L_w(443\text{ nm})]_N$ and $[L_w(550\text{ nm})]_N$ values as a function of chlorophyll concentration. Based on these figures there seems to be little hope of being able to reliably retrieve *C* from a remotely sensed $[L_w(\lambda)]_N$ value. However, in spite of the noise seen in Fig. 22*a* and 22*b*, the *ratios* of normalized water-leaving radiances for different wavelengths can be remarkably well-behaved functions of *C*. Figure 22*c* shows predicted (the line) and observed (dots) values of $[L_w(443\text{ nm})]_N/[L_w(550\text{ nm})]_N$; the agreement between prediction and observation is now rather good. Thus measurement

of $[L_w(\lambda)]_N$ at two (carefully chosen) wavelengths along with application of a bio-optical model for their *ratio* can yield a useful estimate of chlorophyll concentration. Such models are the basis of much remote sensing.

## 43.23 INELASTIC SCATTERING AND POLARIZATION

Although the basic physics of inelastic scattering and polarization is well understood, only recently has it become computationally practicable to incorporate these effects into predictive numerical models of underwater radiance distributions. For this reason as well as because of the difficulty of making needed measurements, quantitative knowledge about the significance of inelastic scattering and polarization in the underwater environment is incomplete.

Inelastic scattering processes are often negligible in comparison to sunlight or artificial lights as sources of underwater light of a given wavelength. However, in certain circumstances transpectral scatter is the dominant source of underwater light at some wavelengths. Figure 23 illustrates just such a circumstance.

Figure 23 shows a measured depth profile from the Sargasso Sea of irradiance reflectance at $\lambda = 589$ nm (yellow-orange light); note that $R(589\text{ nm})$ increases with depth. Because of the fairly high absorption of water at this wavelength $[a_w(589\text{ nm}) = 0.152\text{ m}^{-1}]$ most of the yellow-orange component of the incident solar radiation is absorbed near the

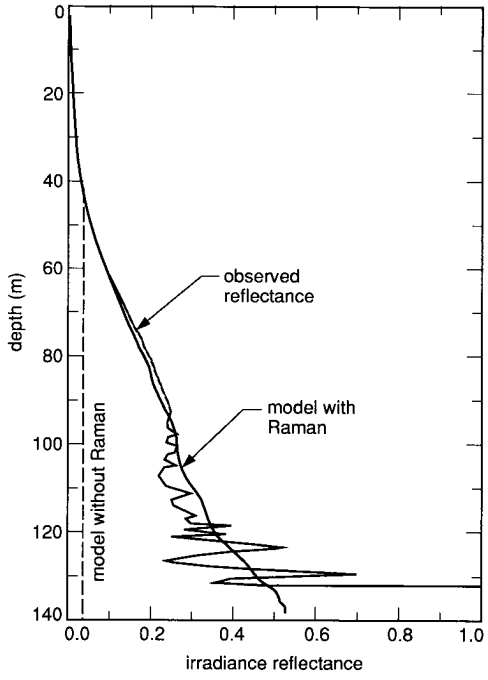


**FIGURE 23** Observed irradiance reflectance $R$ at 589 nm (light line) and values predicted by a model including Raman scattering (heavy line) and omitting Raman scattering (dashed line). (*Redrawn from Marshall and Smith,*[80] *with permission.*)

surface and monochromatic radiative transfer theory shows that the reflectance should approach a value of $R(589\text{ nm}) \approx 0.04$ for the water body of Fig. 22. Calculations by Marshall and Smith[80] explain the paradox. Light of blue-green wavelengths ($\lambda \sim 500$ nm) can penetrate to great depth in the clear Sargasso Sea water [$a_w(500\text{ nm}) \approx 0.026\text{ m}^{-1}$]. Some of this light is then Raman scattered from blue-green to yellow-orange wavelengths providing a source of yellow-orange light at depth. Moreover, since the phase function for Raman scattering is symmetric in the forward and backward hemispheres Raman scattered photons are equally likely to be heading upward [and thus contribute to $E_u(589\text{ nm})$] or downward [and thus contribute to $E_d(589\text{ nm})$] even though most of the blue-green light at depth is heading downward [e.g., $E_d(500\text{ nm}) \gg E_u(500\text{ nm})$]. Thus as depth increases and Raman scattering becomes increasingly important relative to transmitted sunlight as a source of ambient yellow-orange light, $E_u(589\text{ nm})$ and $E_d(589\text{ nm})$ become more nearly equal and the irradiance reflectance $R(589\text{ nm})$ increases. Such an increase is not seen at blue-green wavelengths since $E_d$ transmitted from the surface remains much greater than $E_u$ at great depths. Since Raman scattering is by the water molecules themselves this process is present (and indeed relatively more important) even in the clearest waters. Another oceanographic effect of Raman scattering occurs in the filling of Fraunhofer lines in the solar spectrum as seen underwater; this matter is just now coming under detailed investigation.[81]

Fluorescence by chlorophyll or other substances can be significant if the fluorescing material is present in sufficient quantity. Chlorophyll fluoresces strongly near $\lambda = 685$ nm; this source of red light is responsible[82] for the enhanced reflectance near 685 nm noted in Fig. 21*a*. The spectral signature of fluorescence is a useful tool for analyzing many of the constituents of natural waters.[83]

Relatively little attention has been paid to the state of polarization of underwater light fields.[84] Some use of polarized light has been made in enhancing underwater visibility[85] and it is well established that many oceanic organisms sense polarized light when navigating.[86] Voss and Fry[87] measured the Mueller matrix for ocean water and Quinby-Hunt et al.[88] have studied the propensity of certain phytoplankton to induce circular polarization in unpolarized or linearly polarized light. Kattawar and Adams[89] have shown that errors of up to 15 percent can occur in calculations of underwater radiance if scalar (unpolarized) radiative transfer theory is used instead of vector (polarized) theory.

## 43.24 ACKNOWLEDGMENTS

This paper was written while the author held a National Research Council Resident Research Associateship (Senior Level) at the Jet Propulsion Laboratory, California Institute of Technology. This associateship was supported by the Ocean Biochemistry Program at NASA Headquarters. Final proofing was supported by SRI. Karen Baker, Annick Bricaud, Howard Gordon, Richard Honey, Rodolpho Iturriaga, George Kattawar, Scott Pegau, Mary Jane Perry, Collin Roesler, Shubha Sathyendranath, Richard Spinrad, and Kenneth Voss all made helpful comments on a draft of the paper; their efforts are greatly appreciated.

## 43.25 REFERENCES

1. C. D. Mobley, *Light and Water: Radiative Transfer in Natural Waters,* Academic Press, San Diego, 1994, 592 pp.
2. R. W. Preisendorfer, *Hydrologic Optics,* 6 volumes, U.S. Dept. of Commerce, NOAA, Pacific Marine Environmental Lab., Seattle, 1976, 1757 pp. Available from National Technical Information Service, 5285 Port Royal Road, Springfield, Virginia 22161.

3. A. Morel and R. C. Smith, ''Terminology and Units in Optical Oceanography,'' *Marine Geodesy* **5**(4):335 (1982).
4. N. Højerslev, ''A Spectral Light Absorption Meter for Measurements in the Sea,'' *Limnol. Oceanogr.* **20**(6):1024 (1975).
5. A. Morel and R. C. Smith, ''Relation Between Total Quanta and Total Energy for Aquatic Photosynthesis,'' *Limnol. Oceanogr.* **19**(4):591 (1974).
6. A. Morel, ''Light and Marine Photosynthesis: A Spectral Model with Geochemical and Climatological Implications,'' *Prog. Oceanogr.* **26:**263 (1991).
7. J. T. O. Kirk, ''The Upwelling Light Stream in Natural Waters,'' *Limnol. Oceanogr.* **34**(8):1410 (1989).
8. J. T. O. Kirk, *Light and Photosynthesis in Aquatic Ecosystems,* Cambridge Univ. Press, New York, 1983, 410 pp.
9. R. W. Preisendorfer and C. D. Mobley, ''Theory of Fluorescent Irradiance Fields in Natural Waters,'' *J. Geophys. Res.* **93**(D9):10831 (1988).
10. R. C. Smith and K. Baker, ''The Bio-Optical State of Ocean Waters and Remote Sensing,'' *Limnol. Oceanogr.* **23**(2):247 (1978).
11. H. Gordon, ''Can the Lambert-Beer Law be Applied to the Diffuse Attenuation Coefficient of Ocean Water?,'' *Limnol. Oceanogr.* **34**(8):1389 (1989).
12. C. A. Suttle, A. M. Chan, and M. T. Cottrell, ''Infection of Phytoplankton by Viruses and Reduction of Primary Productivity,'' *Nature* **347:**467 (1990).
13. I. Koike, S. Hara, K. Terauchi, and K. Kogure, ''Role of Submicrometer Particles in the Ocean,'' *Nature* **345:**242 (1990).
14. M. L. Wells and E. D. Goldberg, ''Occurrence of Small Colloids in Sea Water,'' *Nature* **353:**342 (1991).
15. R. W. Spinrad, H. Glover, B. B. Ward, L. A. Codispoti, and G. Kullenberg, ''Suspended Particle and Bacterial Maxima in Peruvian Coastal Water During a Cold Water Anomaly,'' *Deep-Sea Res.* **36**(5):715 (1989).
16. A. Morel and Y.-H. Ahn, ''Optical Efficiency Factors of Free-Living Marine Bacteria: Influence of Bacterioplankton upon the Optical Properties and Particulate Organic Carbon in Oceanic Waters,'' *J. Marine Res.* **48:**145 (1990).
17. D. Stramski and D. A. Kiefer, ''Light Scattering by Microorganisms in the Open Ocean,'' *Prog. Oceanogr.* **28:**343 (1991).
18. A. Alldredge and M. W. Silver, ''Characteristics, Dynamics and Significance of Marine Snow,'' *Prog. Oceanogr.* **20:**41 (1988).
19. K. L. Carder, R. G. Steward, P. R. Betzer, D. L. Johnson, and J. M. Prospero, ''Dynamics and Composition of Particles from an Aeolian Input Event to the Sargasso Sea,'' *J. Geophys. Res.* **91**(D1):1055 (1986).
20. W. M. Balch, P. M. Holligan, S. G. Ackleson, and K. J. Voss, ''Biological and Optical Properties of Mesoscale Coccolithophore Blooms in the Gulf of Maine,'' *Limnol. Oceanogr.* **36**(4):629 (1991).
21. H. Bader, ''The Hyperbolic Distribution of Particle Sizes,'' *J. Geophys. Res.* **75**(15):2822 (1970).
22. I. N. McCave, ''Particulate Size Spectra, Behavior, and Origin of Nepheloid Layers over the Nova Scotian Continental Rise,'' *J. Geophys. Res.* **88**(C12):7647 (1983).
23. C. E. Lambert, C. Jehanno, N. Silverberg, J. C. Brun-Cottan, and R. Chesselet, ''Log-Normal Distributions of Suspended Particles in the Open Ocean,'' *J. Marine Res.* **39**(1):77 (1981).
24. D. G. Archer and P. Wang, ''The Dielectric Constant of Water and Debye-Hückel Limiting Law Slopes,'' *J. Phys. Chem. Ref. Data* **19:**371 (1990).
25. M. Kerker, *The Scattering of Light and Other Electromagnetic Radiation,* Academic Press, New York, 1969, 666 pp.
26. V. M. Zoloratev and A. V. Demin, ''Optical Constants of Water over a Broad Range of Wavelengths, 0.1 Å–1 m,'' *Opt. Spectrosc.* (U.S.S.R.) **43**(2):157 (Aug. 1977).

27. R. W. Austin and G. Halikas, ''The Index of Refraction of Seawater,'' SIO ref. no. 76-1, Scripps Inst. Oceanogr., San Diego, 1976, 121 pp.

28. R. C. Millard and G. Seaver, ''An Index of Refraction Algorithm over Temperature, Pressure, Salinity, Density, and Wavelength,'' *Deep-Sea Res.* **37**(12):1909 (1990).

29. N. G. Jerlov, *Marine Optics,* Elsevier, Amsterdam, 1976, 231 pp.

30. R. W. Spinrad and J. F. Brown, ''Relative Real Refractive Index of Marine Micro-Organisms: A Technique for Flow Cytometric Measurement,'' *Appl. Optics* **25**(2):1930 (1986).

31. S. G. Ackleson, R. W. Spinrad, C. M. Yentsch, J. Brown, and W. Korjeff-Bellows, ''Phytoplankton Optical Properties: Flow Cytometric Examinations of Dilution-Induced Effects,'' *Appl. Optics* **27**(7): 1262 (1988).

32. R. C. Smith and K. S. Baker, ''Optical Properties of the Clearest Natural Waters,'' *Appl. Optics* **20**(2):177 (1981).

33. T. T. Bannister, ''Estimation of Absorption Coefficients of Scattering Suspensions Using Opal Glass,'' *Limnol. Oceanogr.* **33**(4, part 1):607 (1988).

34. B. G. Mitchell, ''Algorithms for Determining the Absorption Coefficient of Aquatic Particles Using the Quantitative Filter Technique (QFT),'' *Ocean Optics X,* R. W. Spinrad (ed.), *Proc. SPIE* **1302:**137 (1990).

35. D. Stramski, ''Artifacts in Measuring Absorption Spectra of Phytoplankton Collected on a Filter,'' *Limnol. Oceanogr.* **35**(8):1804 (1990).

36. J. R. V. Zaneveld, R. Bartz, and J. C. Kitchen, ''Reflective-Tube Absorption Meter,'' *Ocean Optics X,* R. W. Spinrad (ed.), *Proc. SPIE* **1302:**124 (1990).

37. E. S. Fry, G. W. Kattawar, and R. M. Pope, ''Integrating Cavity Absorption Meter,'' *Appl. Optics* **31**(12):2025 (1992).

38. W. Doss and W. Wells, ''Radiometer for Light in the Sea,'' *Ocean Optics X,* R. W. Spinrad (ed.), *Proc. SPIE* **1302:**363 (1990).

39. K. J. Voss, ''Use of the Radiance Distribution to Measure the Optical Absorption Coefficient in the Ocean,'' *Limnol. Oceanogr.* **34**(8):1614 (1989).

40. F. Sogandares, Z.-F. Qi, and E. S. Fry, ''Spectral Absorption of Water,'' presentation at the Optical Society of America Annual Meeting, San Jose, Calif., 1991.

41. W. S. Pegau and J. R. V. Zaneveld, ''Temperature Dependent Absorption of Water in the Red and Near Infrared Portions of the Spectrum,'' *Limnol. Oceanogr.* **38**(1):188 (1993).

42. A. Bricaud, A. Morel, and L. Prieur, ''Absorption by Dissolved Organic Matter of the Sea (Yellow Substance) in the UV and Visible Domains,'' *Limnol. Oceanogr.* **26**(1):43 (1981).

43. C. S. Roesler, M. J. Perry, and K. L. Carder, ''Modeling in situ Phytoplankton Absorption from Total Absorption Spectra in Productive Inland Marine Waters,'' *Limnol. Oceanogr.* **34**(8):1510 (1989).

44. S. Sathyendranath, L. Lazzara, and L. Prieur, ''Variations in the Spectral Values of Specific Absorption of Phytoplankton,'' *Limnol. Oceanogr.* **32**(2):403 (1987).

45. A Morel, ''Optical Modeling of the Upper Ocean in Relation to Its Biogenous Matter Content (Case 1 Waters),'' *J. Geophys. Res.* **93**(C9):10749 (1988).

46. R. Iturriaga and D. Siegel, ''Microphotometric Characterization of Phytoplankton and Detrital Absorption Properties in the Sargasso Sea,'' *Limnol. Oceanogr.* **34**(8):1706 (1989).

47. A. Morel and L. Prieur, ''Analysis of Variations in Ocean Color,'' *Limnol. Oceanogr.* **22**(4):709 (1977).

48. L. Prieur and S. Sathyendranath, ''An Optical Classification of Coastal and Oceanic Waters Based on the Specific Spectral Absorption Curves of Phytoplankton Pigments, Dissolved Organic Matter, and Other Particulate Materials,'' *Limnol. Oceanogr.* **26**(4):671 (1981).

49. O. V. Kopelevich, ''Small-Parameter Model of Optical Properties of Sea Water,'' *Ocean Optics,* vol 1, *Physical Ocean Optics,* A. S. Monin (ed.), Nauka Pub., Moscow, 1983, chap. 8 (in Russian).

50. V. I. Haltrin and G. Kattawar, ''Light Fields with Raman Scattering and Fluorescence in Sea Water,'' Tech. Rept., Dept. of Physics, Texas A&M Univ., College Station, 1991, 74 pp.

51. C. S. Yentsch, ''The Influence of Phytoplankton Pigments on the Color of Sea Water,'' *Deep-Sea Res.* **7:**1 (1960).
52. H. Gordon, ''Diffuse Reflectance of the Ocean: Influence of Nonuniform Pigment Profile,'' *Appl. Optics* **31**(12):2116 (1992).
53. T. J. Petzold, ''Volume Scattering Functions for Selected Ocean Waters,'' SIO Ref. 72–78, Scripps Inst. Oceanogr., La Jolla, 1972 (79 pp). Condensed in *Light in the Sea,* J. E. Tyler (ed.), Dowden, Hutchinson & Ross, Stroudsberg, 1977, chap. 12, pp. 150–174.
54. R. W. Spinrad, J. R. V. Zaneveld, and H. Pak, ''Volume Scattering function of Suspended Particulate Matter at Near-Forward Angles: A Comparison of Experimental and Theoretical Values,'' *Appl. Optics* **17**(7):1125 (1978).
55. G. G. Padmabandu and E. S. Fry, ''Measurement of Light Scattering at 0° by Small Particle Suspensions,'' *Ocean Optics X,* R. W. Spinrad (ed.), *Proc. SPIE* **1302:**191 (1990).
56. Y. Kuga and A. Ishimaru, ''Backscattering Enhancement by Randomly Distributed Very Large Particles,'' *Appl. Optics* **28**(11):2165 (1989).
57. A. Morel, ''Optical Properties of Pure Water and Pure Sea Water,'' *Optical Aspects of Oceanography,* N. G. Jerlov and E. S. Nielsen (eds.), Academic Press, New York, 1974, chap. 1, pp 1–24.
58. K. S. Shifrin, *Physical Optics of Ocean Water,* AIP Translation Series, Amer. Inst. Physics, New York, 1988, 285 pp.
59. G. Kullenberg, ''Observed and Computed Scattering Functions,'' *Optical Aspects of Oceanography,* N. G. Jerlov and E. S. Nielsen (eds.), Academic Press, New York, 1974, chap. 2, pp 25–49.
60. O. B. Brown and H. R. Gordon, ''Size-Refractive Index Distribution of Clear Coastal Water Particulates from Scattering,'' *Appl. Optics* **13:**2874 (1974).
61. J. C. Kitchen and J. R. V. Zaneveld, ''A Three-Layer Sphere, Mie-Scattering Model of Oceanic Phytoplankton Populations,'' presented at Amer. Geophys. Union/Amer. Soc. Limnol. Oceanogr. Annual Meeting, New Orleans, 1990.
62. C. D. Mobley, B. Gentili, H. R. Gordon, Z. Jin, G. W. Kattawar, A. Morel, P. Reinersman, K. Stamnes, and R. H. Starn, ''Comparison of Numerical Models for Computing Underwater Light Fields,'' *Appl. Optics* **32**(36):7484 (1993).
63. A. Morel and B. Gentili, ''Diffuse Reflectance of Ocean Waters: Its Dependence on Sun Angle As Influenced by the Molecular Scattering Contribution,'' *Appl. Optics* **30**(30):4427 (1991).
64. A. Morel, ''Diffusion de la lumière par les eaux de mer. Résultats experimentaux et approach théorique,'' NATO AGARD lecture series no. 61, *Optics of the Sea,* chap. 3.1, pp. 1–76 (1973), G. Halikas (trans.), Scripps Inst. Oceanogr., La Jolla, 1975, 161 pp.
65. O. V. Kopelevich and E. M. Mezhericher, ''Calculation of Spectral Characteristics of Light Scattering by Sea Water,'' *Izvestiya, Atmos. Oceanic Phys.* **19**(2):144 (1983).
66. H. R. Gordon and A. Morel, ''Remote Assessment of Ocean Color for Interpretation of Satellite Visible Imagery, A Review,'' *Lecture Notes on Coastal and Estuarine Studies,* vol. 4, Springer-Verlag, New York, 1983, 114 pp.
67. J. C. Kitchen, J. R. V. Zaneveld, and H. Pak, ''Effect of Particle Size Distribution and Chlorophyll Content on Beam Attenuation Spectra,'' *Appl. Optics* **21**(21):3913 (1982).
68. J. K. Bishop, ''The Correction and Suspended Particulate Matter Calibration of Sea Tech Transmissometer Data,'' *Deep-Sea Res.* **33:**121 (1986).
69. R. W. Spinrad, ''A Calibration Diagram of Specific Beam Attenuation,'' *J. Geophys. Res.* **91**(C6):7761 (1986).
70. J. C. Kitchen and J. R. V. Zaneveld, ''On the Noncorrelation of the Vertical Structure of Light Scattering and Chlorophyll *a* in Case 1 Water,'' *J. Geophys. Res.* **95**(C11):20237 (1990).
71. K. J. Voss, ''A Spectral Model of the Beam Attenuation Coefficient in the Ocean and Coastal Areas,'' *Limnol. Oceanogr.* **37**(3):501 (1992).
72. J. E. Tyler and R. C. Smith, *Measurements of Spectral Irradiance Underwater,* Gordon and Breach, New York, 1970, 103 pp.

73. K. S. Baker and R. C. Smith, ''Quasi-Inherent Characteristics of the Diffuse Attenuation Coefficient for Irradiance,'' *Ocean Optics VI,* S. Q. Duntley (ed.), *Proc. SPIE* **208:**60 (1979).

74. C. D. Mobley, ''A Numerical Model for the Computation of Radiance Distributions in Natural Waters with Wind-Blown Surfaces,'' *Limnol. Oceanogr.* **34**(8):1473 (1989).

75. R. W. Austin and T. J. Petzold, ''Spectral Dependence of the Diffuse Attenuation Coefficient of Light in Ocean Water,'' *Opt. Eng.* **25**(3):471 (1986).

76. D. A. Siegel and T. D. Dickey, ''Observations of the Vertical Structure of the Diffuse Attenuation Coefficient Spectrum,'' *Deep-Sea Res.* **34**(4):547 (1987).

77. S. Sugihara and M. Kishino, ''An Algorithm for Estimating the Water Quality Parameters from Irradiance Just Below the Sea Surface,'' *J. Geophys. Res.* **93**(D9):10857 (1988).

78. H. R. Gordon, O. B. Brown, R. E. Evans, J. W. Brown, R. C. Smith, K. S. Baker, and D. C. Clark, ''A Semianalytic Model of Ocean Color,'' *J. Geophys. Res.* **93**(D9):10909 (1988).

79. S. Sathyendranath and A. Morel, ''Light Emerging from the Sea—Interpretation and Uses in Remote Sensing,'' *Remote Sensing Applications in Marine Science and Technology,* A. P. Cracknell (ed.), D. Reidel, Dordrecht, 1983, chap. 16, pp. 323–357.

80. B. R. Marshall and R. C. Smith, ''Raman Scattering and In-Water Ocean Optical Properties,'' *Appl. Optics* **29:**71 (1990).

81. G. W. Kattawar and X. Xu, ''Filling-in of Fraunhofer Lines in the Ocean by Raman Scattering,'' *Appl. Optics* **31**(30):6491 (1992).

82. H. Gordon, ''Diffuse Reflectance of the Ocean: The Theory of Its Augmentation by Chlorophyll *a* Fluorescence at 685 nm,'' *Appl. Optics* **18:**1161 (1979).

83. J. J. Cullen, C. M. Yentsch, T. L. Cucci, and H. L. MacIntyre, ''Autofluorescence and Other Optical Properties As Tools in Biological Oceanography,'' *Ocean Optics IX,* M. A. Blizard (ed.), *Proc. SPIE* **925:**149 (1988).

84. A. Ivanoff, ''Polarization Measurements in the Sea,'' *Optical Aspects of Oceanography,* N. G. Jerlov and E. S. Nielsen (eds.), Academic Press, New York, 1974, chap. 8, pp. 151–175.

85. G. D. Gilbert and J. C. Pernicka, ''Improvement of Underwater Visibility by Reduction of Backscatter with a Circular Polarization Technique,'' *SPIE Underwater Photo-Optics Seminar Proc.,* Santa Barbara, Oct. 1966.

86. T. H. Waterman, ''Polarization of Marine Light Fields and Animal Orientation,'' *Ocean Optics X,* M. A. Blizard (ed.), *Proc. SPIE* **925:**431 (1988).

87. K. J. Voss and E. S. Fry, ''Measurement of the Mueller Matrix for Ocean Water,'' *Appl. Optics* **23:**4427 (1984).

88. M. S. Quinby-Hunt, A. J. Hunt, K. Lofftus, and D. Shapiro, ''Polarized Light Studies of Marine *Chlorella,*'' *Limnol. Oceanogr.* **34**(8):1589 (1989).

89. G. W. Kattawar and C. N. Adams, ''Stokes Vector Calculations of the Submarine Light Field in an Atmosphere-Ocean with Scattering According to a Rayleigh Phase Matrix: Effect of Interface Refractive Index on Radiance and Polarization,'' *Limnol. Oceanogr.* **34**(8):1453 (1989).